Control of impact crater fracture systems on subsurface hydrology, ground subsidence, and collapse, Mars

Jose Alexis Palmero Rodríguez,[1] Sho Sasaki,[1] James M. Dohm,[2] Ken L. Tanaka,[3] Bob Strom,[2] Jeff Kargel,[3] Ruslan Kuzmin,[4] Hideaki Miyamoto,[2] John G. Spray,[5] Alberto G. Fairén,[6] Goro Komatsu,[7] Kei Kurita,[8] and Victor Baker[2]

Received 24 September 2004; revised 24 February 2005; accepted 21 March 2005; published 15 June 2005.

[1] Noachian layered materials are pervasively exposed throughout the highlands of Mars. The layered deposits, in places many kilometers thick, exhibit impact craters of diverse morphologic characteristics, ranging from highly degraded to pristine, most of which formed during the period of heavy bombardment. In addition, exhumed impact craters, ancient channels, and fluvial and alluvial fans are visible in the layered deposits through MOC imagery. These features are more abundant in Noachian terrains, which indicates relatively high erosion rates during ancient Mars that competed with heavy meteoritic bombardment. The Noachian layered materials are thus expected to contain numerous buried impact craters in various states of preservation. Here, we propose that impact craters (buried and exposed) and associated fracture systems dominate the basement structural fabric of the ancient highlands and that they have significantly influenced the hydrogeology. Diversity in the occurrence of high and low densities of impact craters and associated fracture systems controls the magnitude of the local effects of magmatic-driven hydrothermal activity. In and surrounding the Tharsis region, for example, the formation of chaotic terrains (the source regions of the circum-Chryse outflow channel system) and a large diversity of collapse structures, including impact crater moats and pit chains, appear to be the result of enhanced hydrothermal activity.

Citation: Rodríguez, J. A. P., et al. (2005), Control of impact crater fracture systems on subsurface hydrology, ground subsidence, and collapse, Mars, *J. Geophys. Res.*, *110*, E06003, doi:10.1029/2004JE002365.

1. Introduction

[2] Geologic, paleohydrologic, and geomorphic evidences [e.g., *Craddock and Maxwell*, 1993; *Scott et al.*, 1995; *Baker*, 2001], suggest that Mars has been (and may still be) a planet with abundant groundwater [*Clifford*, 1993; *Carr*, 1996; *Boynton et al.*, 2002; *Mitrofanov et al.*, 2003]. The circum-Chryse outflow channels comprise the most pronounced dissectional signature on the surface of the planet and have been interpreted as having been excavated by a combination of catastrophic [*Carr*, 1996] and noncatastrophic flooding [*Rodriguez et al.*, 2005]. These outflow channels are generally located adjacent to chaotic terrains and extensive areas of plateau subsidence, where moats tend to form around impact craters of various sizes.

[3] *Rodriguez et al.* [2004, 2005] proposed that these regions of plateau subsidence and chaotic terrains formed by the loss of basal hydrostatic support as groundwater pressurized in caverns emerged at the surface. Although control of the subsurface hydrology by tectonic and igneous processes is well documented for Earth and has been widely proposed for Mars [e.g., *Rodriguez et al.*, 2003; *Ogawa et al.*, 2003], the formation and evolution of the putative cavernous aquifers, as well as their control on the surface geomorphology remains largely unsolved.

[4] In this work we investigate possible configurations of extensive fracturing of the Martian surface and subsurface produced by cosmic impacts. We propose that these fracture networks played a very important role in the hydrogeology of Mars, and discuss their role in the formation and evolution of the putative water-filled caverns [*Rodriguez et al.*, 2005], as well as the formation and evolution of a diverse suite of landforms possibly related to cavernous collapse, observed in the plateau regions in the vicinities of the Aureum Chaos and Eos Chasma (Figure 1).

2. Methods

[5] In this work we have constructed digital elevation models (DEM) using data obtained by the Mars Orbiter

[1]Department of Earth and Planetary Science, University of Tokyo, Tokyo, Japan.
[2]Department of Hydrology and Water Resources, University of Arizona, Tucson, Arizona, USA.
[3]U.S. Geological Survey, Flagstaff, Arizona, USA.
[4]Vernadsky Institute, Russian Academy of Sciences, Moscow, Russia.
[5]Planetary and Space Science Center, Department of Geology, University of New Brunswick, Fredericton, New Brunswick, Canada.
[6]Centro de Biología Molecular, CSIC-Universidad Autónoma de Madrid, Madrid, Spain.
[7]International Research School of Planetary Sciences, Pescara, Italy.
[8]Earthquake Research Institute, University of Tokyo, Tokyo, Japan.

0148-0227/05/2004JE002365$09.00

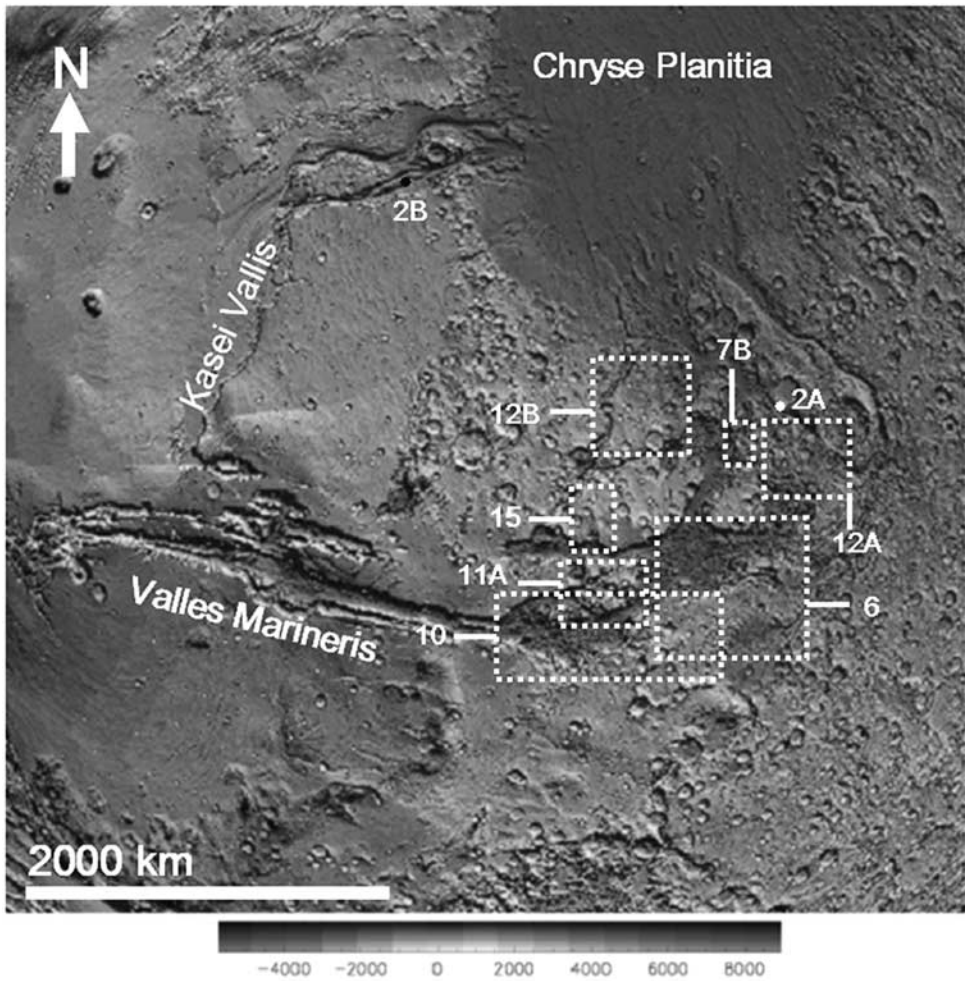

Figure 1. MOLA-based DEM of part of the circum-Chryse region, which includes the location of the Valles Marineris, Noachian plateaus at different stages of subsidence and collapse (Figures 6, 7b, 10, 11a, 12a, 12b, and 15a), and the Chryse basin region. Also shown are the locations of Figure 2a (white dot) and Figure 2b (black dot). In addition, Figure 7a is an inset of Figure 6, Figure 13 is an inset of Figure 12a, and Figure 13c is an inset of Figure 13a. The western Aureum Chaos and the Eos Chasma are shown in the northern part of Figure 6 and the southern part of Figure 10, respectively. See color version of this figure in the HTML.

Laser Altimeter (MOLA) instrument. We have also analyzed the geomorphology of selected visible imagery data obtained by the Mars Global Surveyor MOC (Mars Orbiter Camera) instrument, and day infrared imagery data obtained by the Mars Odyssey THEMIS (Thermal Emission Imaging System) instrument.

[6] The criteria for the selection of the regions discussed in this paper were primarily based on our own regional mapping of eastern circum-Chryse, as well as on the mapping by *Rodriguez et al.* [2005] of the regions located north of the eastern Aureum Chaos, east of the Hydraotes Chaos, and south of the Hydaspis Chaos. The selected regions include zones where subsurface geologic features and structures are clearly exposed as well as regions where the surface has been modified by diverse types of depression.

[7] We also present impact crater statistical analyses based on the crater counts by *Strom et al.* [1992]. In these analyses we have used R plot graphs, which are standard ways of presenting crater size/frequency distributions. They are binned crater diameters normalized to a differential -3 distribution function. Therefore the horizontal line on an R plot is a -3 distribution.

3. Results

[8] In this section we examine and discuss the geomorphologic and topographic characteristics of selected regions in eastern circum-Chryse, and present the results of our impact crater statistical studies.

3.1. Significance of Early Noachian Layered Materials

[9] Layered materials have been identified within Martian terrains, such as those observed in the Arabia Terra region [*Malin and Edgett*, 1999], a proposed site of an ancient, giant impact basin/productive aquifer system [*Dohm et al.*, 2004]. Two sequences of layered materials have been recognized [*Tanaka et al.*, 2004]: (1) Early to Middle

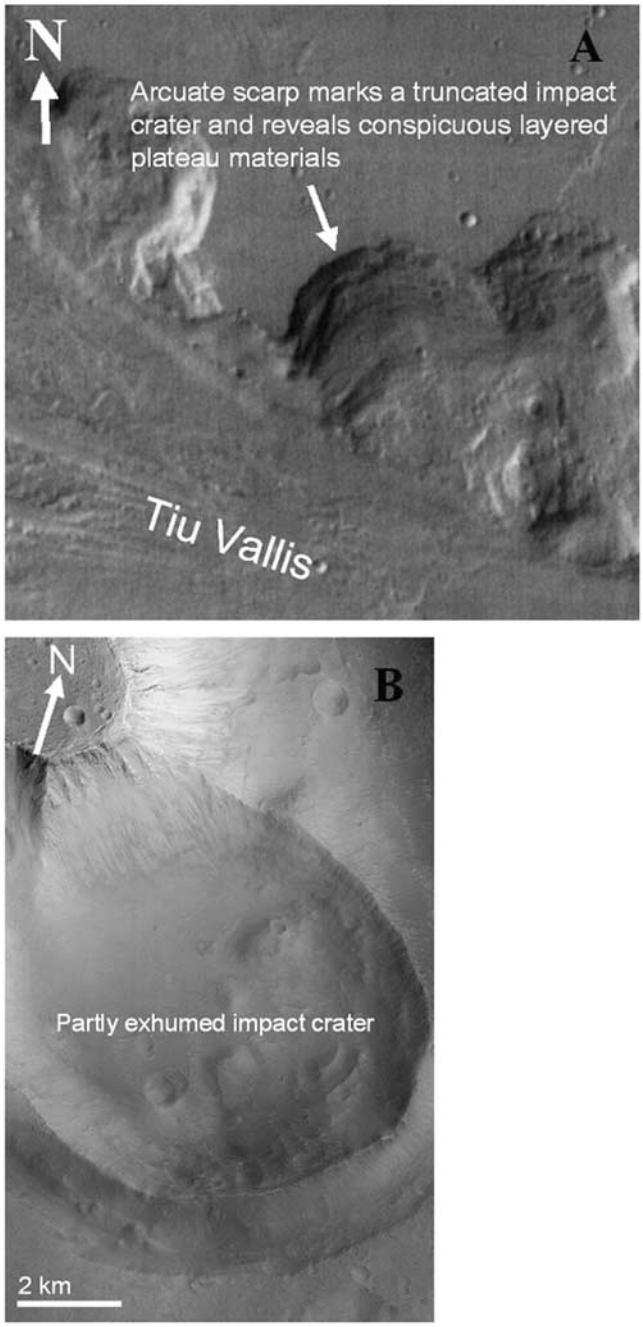

Figure 2. (a) THEMIS day infrared I03883003 subframe centered at 3.91°N, 332.56°E. Image width is 32 km. Region of a Noachian plateau near the Hydaspis Chaos, dissected by the Tiu Vallis. An arcuate scarp, possibly a truncated crater, shows pervasive layering (see Figure 1 for location and context). (b) Mars Global Surveyor Mars Orbiter Camera image 34504 subframe centered at 24.3°N, 298.5°E. Shown is an exhumed impact crater at the base of a mesa in the Kasei Valles system (see Figure 1 for location and context).

Noachian, relatively indurated layers exposed in crater and channel walls (e.g., Figure 2a), and (2) Late Noachian and younger friable layers superposing degraded craters and commonly eroded into yardangs.

[10] These layered materials may have resulted from a variety of geological processes [e.g., *Scott and Tanaka*, 1986; *Schultz and Lutz*, 1988; *Moore*, 1990; *Tanaka*, 2000; *Hynek et al.*, 2003], including fluvial, alluvial, colluvial, eolian, debris flow, subaqueous, tectonic, and impact activities, as well as the emplacement of volcanic materials. Secondary diagenetic processes, such as burial diagenesis due to heat in presence of water, may have contributed to the formation or destruction of layered materials [*Cohen and Treiman*, 1999; *Fuks et al.*, 1995].

[11] The extremely Early Noachian is a geologic period referred to by some authors as the "pre-Noachian" [e.g., *Frey*, 2004]. Mapping of "quasi-circular depressions" (QCDs) by *Frey* [2004] indicates that the "pre-Noachian" may have extended for as long as from 4.6 billion years ago until 4.2 billion years ago (the base of the Early Noachian).

[12] *Dohm et al.* [2001, 2004] suggest that during the "pre-Noachian" these layered materials were deposited in ancient paleobasins, and proposed that their infilling materials may have sourced from surrounding topographically higher regions, such as paleo-orogenic complexes, plateaus, rims of craters or basins, volcanic edifices, and/or fissure systems. This would require that the putative source regions have been destroyed or highly degraded. This proposition is consistent the mapping of QCDs by *Frey* [2004], which indicates that during the "pre-Noachian" a large number of impacts basins and impact craters were buried to depths ranging from <1 km to 6 km (based on *Garvin et al.* [2000]). These observations suggest that during the "pre-Noachian" more Earth-like erosional/depositional rates prevailed [e.g., *Baker et al.*, 2002; *Fairén et al.*, 2003].

[13] We propose much of the layered "pre-Noachian" basement and plateau materials may have been deposited in ancient paleobasins, prior to reworking during the heavy bombardment into the Early Noachian and later surfaces [e.g., *Scott and Tanaka*, 1986]. This view is in sharp contrast to the way the Martian crust was viewed prior to the Mars Global Surveyor (MGS) as being composed primarily of fractured primordial basement rocks and an overlying impact-generated megaregolith layer [e.g., *Carr*, 1996].

3.2. Geologic Significance of Buried Impact Craters and Associated Tectonic Fabrics

[14] Radial and concentric fault systems have been documented about the site of some major cosmic impacts [e.g., *Abineri*, 1995; *von Dalwigk*, 2003]. Impact-induced tectonic structures have been recognized on Earth and consist predominantly of strike-slip and listric extensional structures [*Osinski and Spray*, 2003]. In this section we discuss some of the evidence for abundant buried impact crater populations on Mars, the multiple configurations of buried impact crater fracture networks, and their thermal and hydrogeologic significance.

3.2.1. Buried Impact Craters on Mars

[15] The fact that layered deposits exhibit exhumed impact craters (Figure 2b) as well as ancient channels, fluvial deposits, and alluvial fans, as observed using MOC imagery [e.g., *Malin and Edgett*, 2000], and the fact that these features are more abundant in Noachian terrains, suggest relatively high resurfacing rates contemporaneous with heavy meteoritic bombardment.

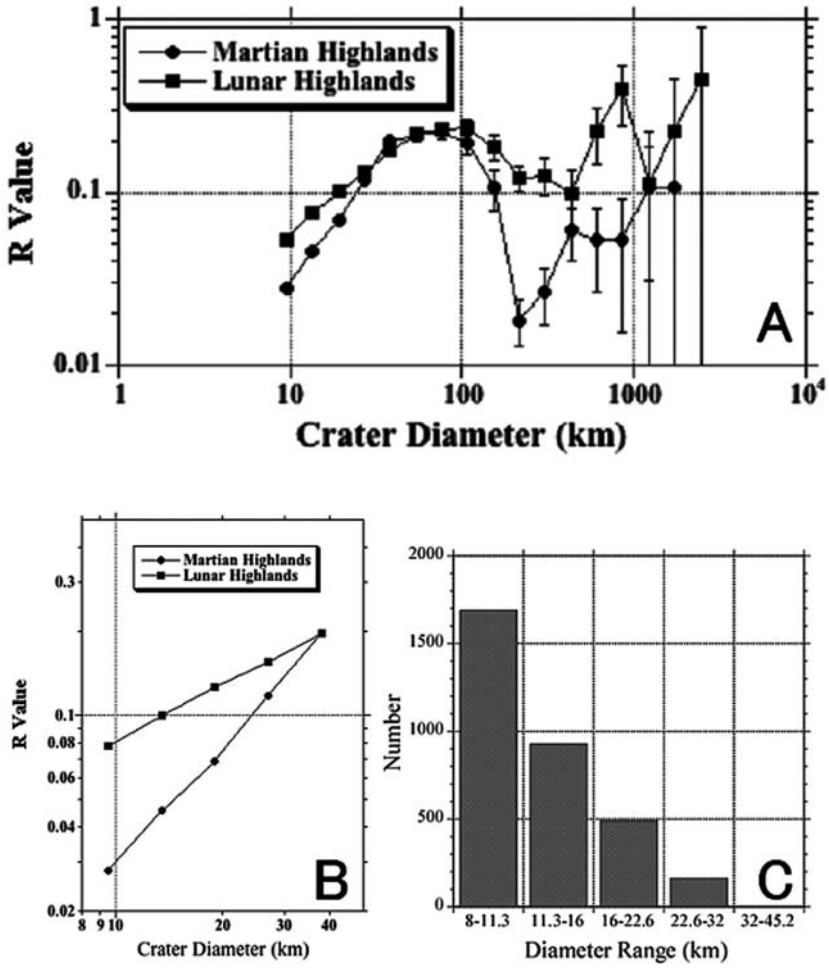

Figure 3. (a) R plot of the size/frequency distributions of the lunar and Martian highlands. The total number of craters used in the counts is about 6285 for the Moon and 2804 for Mars [*Strom et al.*, 1992]. The cratering record used in this study represents the period of Late Heavy Bombardment that ended about 3.8 Ga. For this study any difference in the cratering rate between the Moon and Mars is irrelevant. The crater number density and departure of the Martian distribution function from that on the Moon at equivalent diameters are the relevant observations. Since the Martian crater density decreases at smaller diameters compared to the lunar density, they must have been obliterated by intercrater plains formation on Mars (intercrater plains in the lunar highlands are negligible but are abundant on Mars). The difference is therefore a measure of the crater obliteration (burial) on Mars due to intercrater plains formation. (b) Crater size distribution for the Martian highlands at diameters from 8 to 45 km and the lunar crater size distribution over the same diameter range normalized to the 32 to 45 km size bin where the Martian curve begins to deviate from the lunar curve. The crater loss on Mars due to obliteration by intercrater plains is simply the difference in number of craters between the lunar and Martian curve between 8 and 32 km diameter normalized to the area of Mars. (c) Histogram showing the number of craters lost in each size bin by burial or destruction over an area of 8.8×10^6 km^2 in the Martian highlands.

[16] The crater size/frequency distribution of the Martian highlands can be used to estimate the number of buried or destroyed craters. Figure 3a shows a relative size-frequency (R) plot of the craters in the lunar and Martian highlands. The Martian distribution has a steeper slope at diameters less than about 32 km diameter compared to the Moon. The probable reason is that a relatively large number of craters have been obliterated by intercrater plains on Mars, but not on the Moon. Intercrater plains on the Moon are rare.

[17] Figure 3b shows the crater size distribution for the Martian highlands at diameters from 8 to 45 km and the lunar crater size distribution over the same diameter range normalized to the 32 to 45 km size bin where the Martian curve begins to deviate from the lunar curve. This does not mean there has been no crater loss at larger diameters. There clearly has been burial of larger craters. However, the larger degraded craters are more easily recognized and counted in the crater statistics as degraded craters or rings similar to those in the lunar maria. The difference between the two curves is an estimate of the number of buried or destroyed craters due to intercrater plains formation at diameters less than about 32 km. Figure 3c is a histogram showing the number of craters lost in each size bin by burial or destruction over an area of 8.8×10^6 km^2 (or ~6% of the

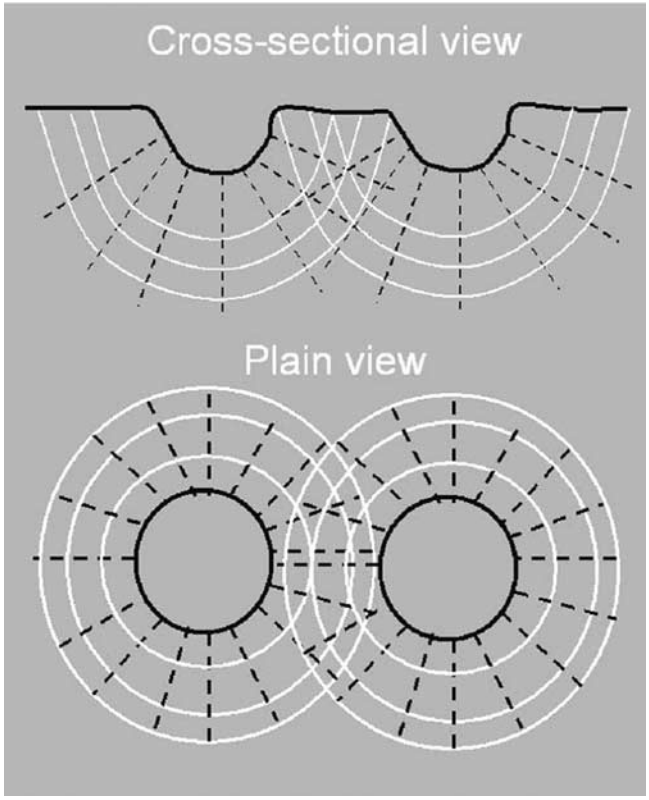

Figure 4. Diagrams showing the (top) cross-sectional and (bottom) plain views of the peripheral fault systems around impact craters (white concentric faults and dashed black radial faults).

total surface of Mars). Within the size range of 8 to 32 km diameter the total number of lost craters is over 3200. In addition, global mapping by *Frey* [2004] has revealed the more than 500 QCDs larger than 200 km in diameter, as well as a small population of 10 very large buried basins (D = 1300–3000 km) on Mars. Thus there are surely numerous buried impact craters on Mars, particularly in ancient (''pre-Noachian'' to Middle Noachian) paleobasin infill materials and buried basement.

3.2.2. Impact Crater Fracture Networks

[18] Because of the expected wide range in the dimensions of paleobasins, and in local to regional spatial as well as temporal variations in erosional and depositional rates, subsurface plateau and plains geologic materials are expected to include numerous buried impact craters in various preservational states and densities. For example, periods of high degradation and rapid and/or extended basin burial will have resulted in the formation of layered sequences with relatively less abundant buried impact crater populations. On the other hand, periods of low degradation and slow and/or short-lived surface burial are expected to result in layered deposits with relatively higher abundances of buried crater populations. We propose that the frequency of buried craters should vary with depth and from one region to another.

[19] We have observed that interconnecting structurally controlled troughs about surface and buried impact craters extend to approximately 1/3 of the craters' diameters outward from the rims (see section 3.3.1.1). These troughs may represent regions peripheral to impact craters where there is a dense packing of fault systems [e.g., *Abineri*, 1995; *von Dalwigk*, 2003]. *Ormö and Blomqvist* [1996] in their study of the magnetic structure of the marine Tvären Bay impact crater (Sweden) estimated the shape, depth and extension of the crater and the surrounding region of the basement that was fractured by the impact. They concluded that the fractured bedrock extended about 1/2 of the crater's diameter outward from the rim. *Gurov and Gurova* [1982] come to another conclusion after studying the Siberian Elgygytgyn structure. They found that increased fracturing extended approximately 1 crater diameter outward from the rim. We have called this value ''distance of high peripheral interconnectivity,'' and in this study we assume it to be a variable ranging from 1/3 to about 1 crater diameter from the rim, and the respective densely fractured regions ''regions of high peripheral interconnectivity.''

[20] On Earth, ground-based mapping of the larger (>100 km diameter) impact structures has revealed the development of radial and concentric fracture-fault systems beyond collapsed transient cavities. In the case of Sudbury, concentric faults are developed to approximately twice the transient cavity diameter (i.e., out to ~250 km, given a proposed collapsed transient cavity diameter of ~130 km), and radial faults out to at least the collapsed transient cavity margins [*Spray and Thompson*, 1995; *Spray*, 1998; *Spray et al.*, 2004]. These fracture-fault systems have been sites for friction melt (pseudotachylyte) generation, impact melt injection and postimpact fluid flow. At Haughton, which is a smaller structure, concentric faults extend beyond the ~16-km-diameter collapsed transient cavity out to ~24 km diameter, i.e., 4 km additional radius [*Osinski et al.*, 2005]. These faults, along with radials, have been conduits for hydrothermal fluid flow and mineralization during cooling of the impact melt sheet [*Osinski et al.*, 2001]. These terrestrial examples show at least the concentric fracture-fault systems extending 1–2 times the collapsed transient cavity radii.

[21] We propose intermingling concentric and radial fracture systems (Figure 4) associated with multiple surface and/or buried impact craters will have resulted in complex impact crater fracture networks in uncompacted plateau and plains geologic materials. Impact crater fracture networks associated with closely clustered (within their distance of high peripheral interconnectivity) populations of surface and/or buried impact craters will form high fracture density regions. On the other hand, impact crater fracture networks associated with sparsely spaced populations of surface and/or buried impact craters will produce low fracture density regions.

[22] The configurations of high and low fracture density subsurface zones for a given uncompacted subsurface zone may include (1) relatively thick and laterally extensive high fracture density regions (Figures 5a and 5b) and/or (2) alternating, relatively thin and laterally extensive, high and low fracture density regions (Figures 5c and 5d).

[23] As such, we propose that impact crater fracture networks are very significant features of the Martian subsurface geology, and may even dominate the basement structural fabric in the ancient crustal regions. Stratigraphic contacts and fault planes may interconnect or isolate regions of high and low fracture density, depending on their respective permeabilities.

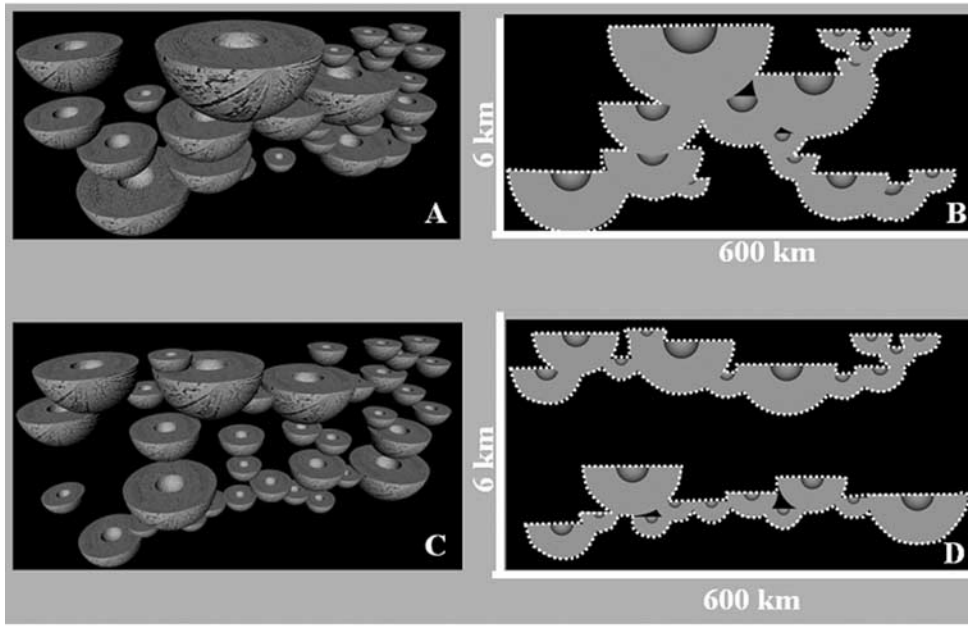

Figure 5. Variables such as the number, size, and distribution of surface and buried impact craters, as well as the thickness of the infilling geologic materials for a given paleobasin, will result in multiple and very complex 3-D spatial configurations of the crater-related fracture networks. In a realistic geologic scenario, there is possibly a combination of multiple configurations, although some are more likely to be dominant in certain geologic settings or periods. For example, (a) three-dimensional representation a randomly distributed buried, and some surface, impact craters to a depth of 6 km (hollow hemisphere within the patterned solid volumes), as well as their associated regions of high peripheral interconnectivity extending about 1 crater diameter away from each crater rims (patterned solid volumes). The impact crater diameters range from 10 km to 50 km, with a significant population of impact craters between 30 and 50 km in diameter. (b) Cross-sectional view of the impact crater population shown in Figure 5a. All the impact craters with high peripheral interconnectivity regions that do not overlap have been removed. The dotted white line demarks a relatively thick and laterally extensive high fracture density region. We propose that this type of configuration of high fracture density regions may underlie some of the Martian intercrater plains as well as some of the plateau regions formed by the infill of extremely ancient and deep paleobasins during the heavy bombardment. After the heavy bombardment a similar crater fracture network configuration may form in relatively small and shallow basins with a population of predominantly small surface and buried impact craters. (c) Three-dimensional representation of randomly distributed buried, and some surface, impact craters to a depth of 6 km (hollow hemisphere within the patterned solid volumes), as well as their associated regions of high peripheral interconnectivity extending about 1 crater diameter away from each crater rims (patterned solid volumes). The impact crater diameters range from 10 km to 50 km, but with a dominant population of impact craters 10–20 km in diameter. (d) Cross-sectional view of the impact crater population shown in Figure 5c. All the impact craters with high peripheral interconnectivity regions that do not overlap have been removed. The dotted white line demarks multiple levels of relatively thin and laterally extensive high fracture density regions (dashed white lines). We propose that this type of configuration of high fracture density regions may exist in very rapidly infilled basins, particularly after the heavy bombardment.

[24] Interconnection within and among regions of high fracture density and crustal cryolithospheric destabilization in these interconnected regions will be enhanced by subsequent endogenic- or exogenic-induced tectonism. For example, magmatic and tectonic activity, particularly related to the evolution of the Tharsis uplift [e.g., *Anderson et al.*, 2001; *Dohm et al.*, 2001], and/or in regions of possible plate tectonism during the extremely ancient period of Mars [e.g., *Baker et al.*, 2002; *Dohm et al.*, 2002; *Fairén et al.*, 2002, 2003; *Fairén and Dohm*, 2004], may have disrupted regions of crater fracture networks, resulting in additional lateral and vertical variations in the density and distribution of fractures, and may have resulted in the reorientation of preexisting fracture systems into random patterns. A similar relation is expected in and surrounding the Elysium rise, related to its independent but analogous evolution.

3.3. Crater Fracture Networks and the Surface Landforms of Mars

[25] Because ice and porous geologic materials have low thermal conductivity, in regions of Mars that are desiccated or that are or were icy [*Tanaka*, 2000; *Clifford and Parker*,

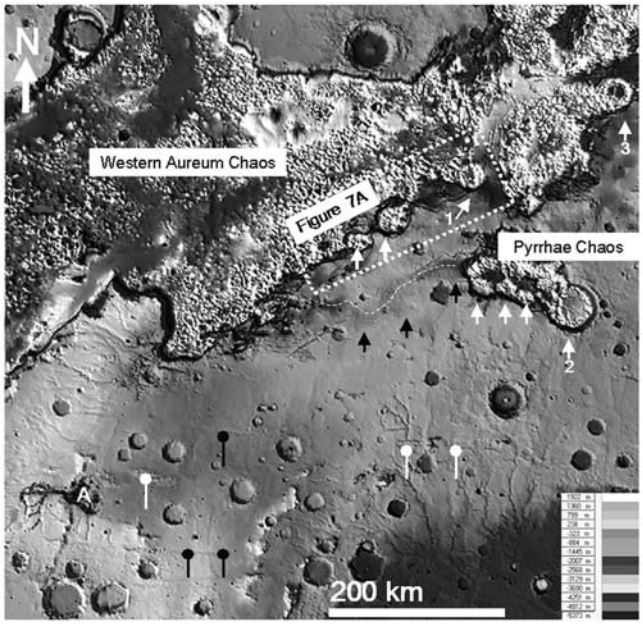

Figure 6. MOLA-derived DEM of the western Aureum Chaos and surrounding plateau highlands. Region centered at 11.65°S, 327°E. Shown is a northeast trending depression (dashed white line) that extends from the margins of the western Aureum Chaos to the margins of the Pyrrhae Chaos. The margins of this depression are arcuate and fracture-bounded in places (black arrows), which is consistent with the hypothesized subsidence of upper crustal materials over buried impact craters. Depressions (white arrows) resembling destroyed buried impact craters are also interpreted to mark subsidence and collapse over buried craters. West trending grabens (black pointers) are associated with a west trending system of ridges (white pointers). The orientation of the graben systems is radial about the Tharsis rise, suggesting that they are the result of the growth of the Tharsis rise. The ridge system may be composed of the erosional remnants of dikes emplaced over long distances along the fault systems. The surface of the plateau is extensively dissected by channel systems, which appear to be associated with collapsed regions in places (A). This suggests a complex tectonomagmatic and hydrologic history [e.g., *Komatsu et al.*, 2004]. The dotted white rectangle depicts the Chain of quasi-circular depressions shown in Figure 7a (see Figure 1 for location and context). See color version of this figure in the HTML.

2001], but remain largely frozen during a given heat flow, regions of high fracture density would also be regions of lower thermal conductivity. Therefore these regions would have a higher thermal gradient compared to regions of low fracture density. On the other hand, meltwater derived from ice [*Komatsu et al.*, 2000], or from subsurface aquifers where groundwater may be stable, will cause more efficient hydrothermal transport of heat along fracture planes by hydrothermal convection, than through the rock matrix, and thus areas of high fracture density would be loci of higher thermal conductivity. As a consequence, we propose that crater fracture networks will result in highly nonisotropic heat flow distribution (leading to episodic Tharsis activity [*McKenzie and Nimmo*, 1999; *Dohm et al.*, 2001; *Chapman and Tanaka*, 2002]), including lateral as well as heterogeneous vertical heat transfer within uncompacted plateau and plains subsurface geologic materials. In this section we discuss Martian surface landforms that may have been produced by enhanced hydrothermal activity within regions of high fracture density.

3.3.1. Crater Fracture Networks and the Formation and Evolution of Confined Cavernous Systems

[26] *Rodriguez et al.* [2005] have proposed that the undulating, warped, and densely fractured surfaces of highland regions east of Valles Marineris (located north of the eastern Aureum Chaos, east of the Hydraotes Chaos, and south of the Hydaspis Chaos) resulted from extensional surface warping related to ground subsidence, caused when pressurized water confined in subterranean caverns was released to the surface. Water emanations formed crater lakes and resulted in channeling episodes involved in the excavation of Ares, Tiu, and Simud Valles of the eastern part of the circum-Chryse outflow channel system. Ancient cratered highland and basin materials that underwent large-scale subsidence grade into densely fractured terrains. Collapse of rock materials in these regions resulted in the formation of chaotic terrains, which occur in and near the headwaters of the eastern circum-Chryse outflow channels. They observe that the size, orientation, and shape of the knobs, ridges, and mesas, which form the eastern Aureum Chaos, are largely nonchaotic, and preserve surface landforms and structures, which is consistent with relatively shallow and nonturbulent collapse, and basement structural control, both related to impact craters [*Banerdt et al.*, 1992] and surface extensional tectonic fabrics [*Banerdt et al.*, 1992]. Next, we investigate the formation and evolution of these putative caverns.

3.3.1.1. Subsurface Architecture of the Subterranean Cavernous Systems

[27] A system of two northeast trending depressions (Figure 6) occurs within the Late Noachian subdued cratered highlands [*Rotto and Tanaka*, 1995], forming the southern margin of eastern Aureum Chaos. The one shown by the dashed white line in Figure 6 extends from the margin of western Aureum Chaos to Pyrrhae Chaos, resembling those observed in the Noachian plateau north of the Aureum Chaos (interpreted by *Rodriguez et al.* [2004, 2005] to be the result of ground subsidence over caverns).

[28] The northern one (marked by the dotted box in Figure 6) occurs along the margin of western Aureum Chaos (Figures 6 and 7a), and consists of a chain of quasi-circular pits interconnected by troughs (black pointers in Figure 7a). These troughs extend approximately 1/3 of the pits' diameters (see section 3.2.2).

[29] In Figure 7a, pit A is filled with chaotic material, and it is approximately 3 km deeper than the adjacent highland margin. The southwest part of pit B consists of chaotic material, whereas the northeast part consists of a system of northeast trending ridges, which suggests that the progressive breakup and degradation of the ridge systems may have resulted in the formation of the chaos covering the southwest part. Pit C has a smooth and fractured surface, which is texturally continuous with the adjacent plateau surface. Pit D has a shallow and chaotic floor, partly surrounded by a scarp.

[30] In a highly fractured and blocky highland remnant, north of the pit chain (Figure 7a), there is a northeast trending elongate fracture bounded depression with a lateral gorge and an adjacent pit. This region resembles the previously mentioned pit chain. Another system of northeast trending depressions, which resemble the Aureum pit chain (Figure 7b), occurs within the Late Noachian subdued cratered unit [*Rotto and Tanaka*, 1995], located north of the Aureum Chaos, south of the Hydaspis Chaos and east of the Hydraotes Chaos. This system of depressions consists of fracture-bounded quasi-circular depressions, elongate depressions, and a partially destroyed crater. The northeast margin of this crater has been destroyed by a trough, which resembles the troughs between the pit chain shown in Figure 7a.

[31] Suggested mechanisms regarding the origin of 1 to 4 km in diameter pits forming chains in the western hemisphere of Mars include: Collapsed lava tubes (e.g., NASA/JPL, available online at http://photojournal.jpl.nasa.gov/catalog/, ID number PIA03836); dike swarms [*Mège and Masson*, 1996, 1997; *Liu and Wilson*, 1998; *Mège*, 1999; *Montesi*, 1999; *Scott et al.*, 2000, 2002; *Gibbons et al.*, 2001; *Wilson and Head*, 2001, 2002; *Scott and Wilson*, 2002]; dike swarms possibly associated with collapsed magma chambers [*Mège et al.*, 2000, 2002, 2003]; karst dissolution [*Spencer and Fanale*, 1990]; fissuring beneath loose material [*Tanaka and Golombek*, 1989; *Horstman and Melosh*, 1989; *Banerdt et al.*, 1992; *Tanaka*, 1997]; and dilational faulting related to crustal extension in regions of stratigraphy of varying mechanical strength [*Ferrill and Morris*, 2003; *Ferrill et al.*, 2003; *Sims et al.*, 2003; *Wyrick et al.*, 2003, 2004]. The pits shown in Figure 7 are between 30 km and 40 km in diameter. In the adjacent plateau regions there is a lack of direct evidence for dike swarms (such as cinder cones, lava flows and maar eruptions) as well as for significant crustal extension.

[32] The pits occurrence in plateau zones hypothesized to be underlain by systems of extensive caverns [*Rodriguez et al.*, 2005] suggests that the Aureum pit chain and the fracture-bounded quasi-circular depressions, shown Figure 7, represent zones of cavernous collapse. The lack of spectroscopic evidence for carbonates in these regions, suggests that karst dissolution did not play a significant role in the formation of the caverns, although a very thin layer of dust would obscure or distort the spectral signature of the underlying terrain.

[33] Collapsed impact craters are clustered in plateau regions apparently modified by cavernous collapse (see section 3.3.4). *Rodriguez et al.* [2005] recognize transitional morphologies of highly degraded, to mostly destroyed impact craters within the Aureum chaos and the surrounding highlands. Some of the highly destroyed impact craters preserve some diagnostic features such as rim ridges or ejecta blanket (e.g., Figure 6, yellow arrows 1, 2), and some resemble moated impact craters (e.g., Figure 6, yellow arrow 3), whereas the mostly destroyed impacts consist of regions within chaotic terrains where the distribution of knobs and mesas mark the impact crater like outlines and their peripheral fault systems (e.g., Figure 6, yellow arrow 3). Some of these highly degraded impact craters strongly resemble pits A and B in Figure 7a, as well as other pits within Pyrrhae Chaos.

[34] These observations suggest that these pits may be formed by surface subsidence over buried impact craters. This is consistent with the fact that pit C in Figure 7a and some of the aligned depressions in Figure 7b resemble the quasi-circular depressions mapped by *Frey* [2004] and mapped by him as buried impact craters. We propose that the hypothesized extensive caverns in eastern circum-Chryse primarily formed by the removal of subsurface geologic materials from within and around buried impact craters in subsurface regions of high fracture density.

3.3.1.2. Groundwater Enrichment of Buried Impact Craters and Associated Tectonic Fabrics

[35] The existence of valley networks dissecting crater rims in the ancient Noachian highlands [*Carr*, 1996, 2002] suggests that crater interior deposits may have contained large amounts of regularly recharged water-enriched sediments. As a consequence, Noachian impact craters are likely surface regions where lakes may have formed during geologic periods when warmer and wetter climatic conditions prevailed.

[36] During the Late Noachian-Early Hesperian, the formation and thickening of the cryolithosphere resulted in confinement of a large population of buried Noachian craters (see section 3.2.1) within permafrost, and possibly in the total or partial freezing of the groundwater rich regions [*Clifford*, 1993; *Clifford and Parker*, 2001]. We propose that the interior deposits, within a large number of Noachian (and "pre-Noachian") buried impact craters and associated structures, are likely to be, or have been, ice and/or liquid groundwater enriched zones within the Martian cryolithosphere, wherever ground ice is, or has been, stable [*Clifford*, 1993; *Clifford and Parker*, 2001], due to elevated hydraulic conductivity and storage.

3.3.1.3. Transition of Regions of High Fracture Density Into Caverns Filled With Pressurized Water

[37] Basal warming controlled by regional tectonic fabrics, such as in the case of dikes intruded along the Tharsis rise peripheral fault systems, or controlled by large-scale regional intrusive magmatism, may have resulted in episodes of high heat flow within the Martian cryolithosphere.

[38] If meltwater was produced or groundwater was stable within the subsurface during a given episode of high heat flow, then control of hydrothermal circulation by the faults radiating from individual craters within regions of high fracture density, implies that heat flow will tend to converge into the base of the impact crater-infill deposits. Depending on thermal states, these regions may experience either ice enrichment by freezing of hydrothermal fluids, or preferential warming and melting of interior ice-enriched layered deposits and exterior ice within peripheral porous materials due to the heat advected by the hydrothermal flux.

[39] Within these regions of high fracture density, the production of large volumes of meltwater will result in greater hydrothermal circulation and rapid fluid flows through the densely packed fracture networks. Regional hydrothermal circulation may have resulted in fracture enlargement (or constriction if materials precipitated out of solution), forming conduits that allowed subsurface migration of volatiles as well as escape to the Martian

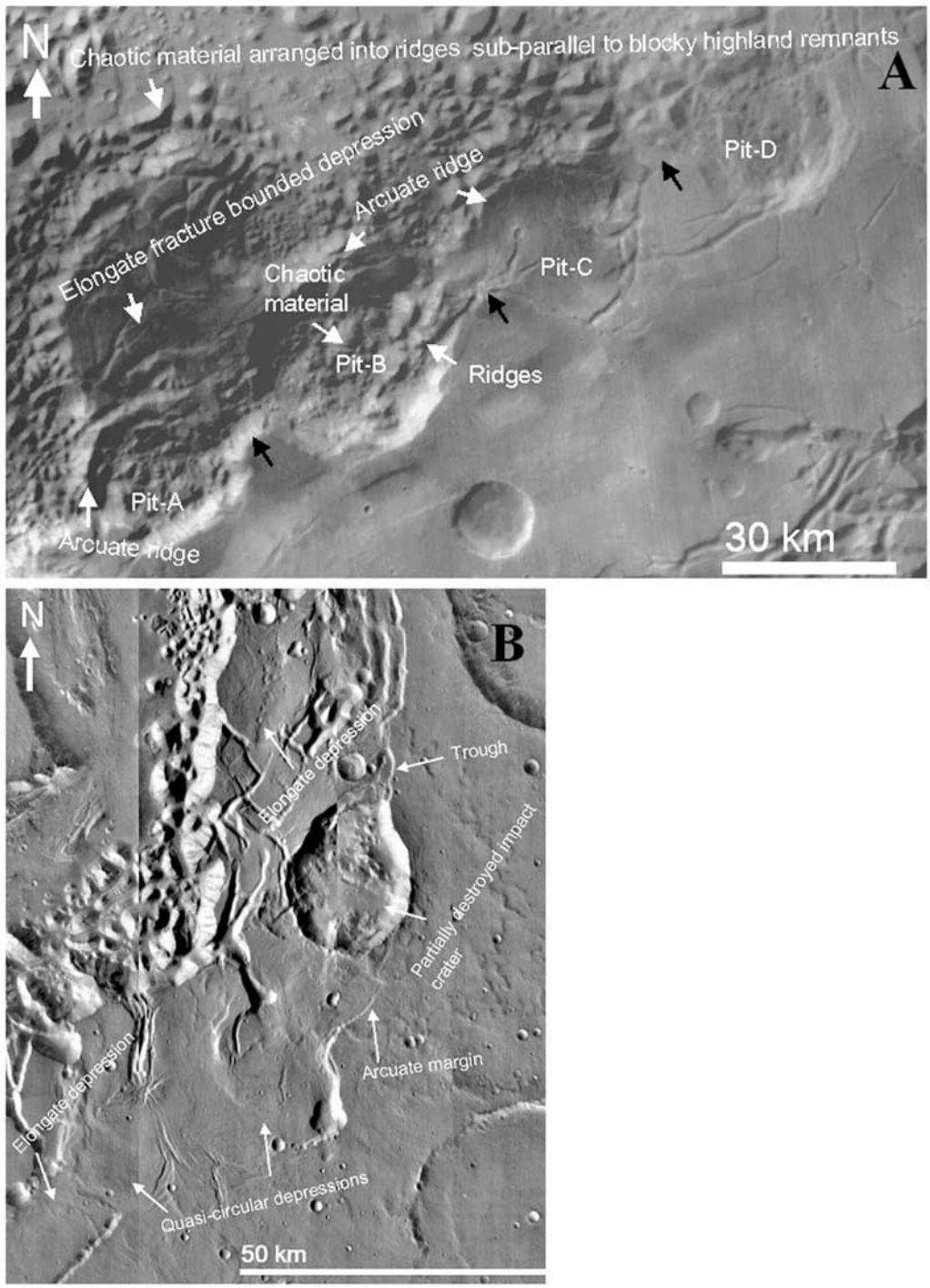

Figure 7. (a) Digitally enhanced Viking mosaic of a chain of interconnected pits. Region centered at 8.68°S, 329.48°E. We interpret this region to have formed through collapse over cavernous systems. The patterns of collapse suggest that the formation of the caverns involved the excavation of interconnected impact craters buried at different depths (see Figure 6 for location and context). (b) THEMIS day infrared digital composite of part of the northern subsided plateau region [*Rodriguez et al.*, 2005], north of the Aureum Chaos and west of the Hydraotes Chaos. Region centered at 2.04°N, 329.02°E. Northeast trending system of quasi-circular depressions, elongate depressions, and a partially destroyed impact crater reveals how the subsurface erosion along the tectonic fabrics interconnecting impact craters may have played an important role in the formation of the putative cavernous systems.

surface and atmosphere. The efficiency of erosion and transport of rock debris along these subsurface conduits could be enhanced by carbon-dioxide-assisted flow related to saturated brine depressurization and exsolution, which can help explain outflow channel-forming floods and northern plains deposits [*Baker et al.*, 1991, 2000; *Tanaka et al.*, 2003]. This is because carbon dioxide exsolution may increase the turbulence of the flow, and because associated fluid expansion may result in the disintegration of geologic materials [*Kling et al.*, 1994; *Mader et al.*, 1994; *Zhang et al.*, 1997; *Zhang*, 1998].

[40] Hydrologic activity within regions of high fracture density may have resulted in the dissolution and/or precipitation of soluble geologic materials along fracture systems, which may result in variations in subsurface permeability and salinity. Decreased permeability may result in the formation of totally or partially confined aquifers; increased permeability will enhance fluid mobility, and thus subsurface erosion. Incremented salinity will result in groundwater being stable at notably negative temperatures, so that it will be able to migrate through colder cryolithospheric regions, and/or form cryopegs within and/or at the base of the Martian cryolithosphere [e.g., *Kuzmin and Zabalueva*, 1998].

[41] We propose that deformation and removal of crater geologic materials may result in the formation of water-filled cavities interconnected by crater fracture networks reworked into conduits, forming extensive caverns. Other processes, such as the removal of subterranean geologic materials and volatiles by subsurface flow [*Carr*, 1996], magmatic-induced segregation of the water phase within the cryolithosphere into discrete subsurface cavities [*Rodriguez et al.*, 2003; *Ogawa et al.*, 2003], clathrates dissociation, and incongruent salt melting/dehydration, may have led or contributed to the formation subterranean caverns partly or completely filled with water [*Boston et al.*, 2001; *Rodriguez et al.*, 2004, 2005].

[42] Initial groundwater pressurization may have been induced by water vapor circulation and possibly by clathrate dissociation [*Komatsu et al.*, 2000], if surrounding ice-saturated cryolithosphere and/or other impermeable geologic materials confined the hydrothermal systems. For example, groundwater-silicate reactions, as well as additions of magmatic and deep crustal gases to groundwater, generating mineral-laden and gas-rich brines, salt hydrates, and clathrate hydrates, could result in cementation by ice and salts in the upper and/or surrounding permafrost layer, potentially creating an impermeable caprock and hence a confined aquifer [*Carr*, 1979; *Max and Clifford*, 2000; *Clifford and Parker*, 2001].

[43] Alternatively, pressurized groundwater systems will result even if there is not complete confinement, but the water dissipation rate after pressurization is relatively low. Further additions of gases, magmatic activity driven heat flow reactivation/increase and/or surface loading above these systems may create overpressurization. Mechanisms of confinement as well as the degree of pressurization of groundwater within the putative caverns are likely to vary significantly depending on the local tectonomagmatic history and geologic period of formation.

[44] We conclude that water-filled caverns may have formed in some regions of high fracture density within water-enriched zones of the Martian cryolithosphere. Within these water-filled caverns, the transient balance between the hydrostatic pressure exerted by the confined groundwater and the lithostatic pressure exerted by the confining geologic materials [*Rodriguez et al.*, 2004, 2005] may result in these caverns being highly unstable. We have called these subsurface hydrogeologic systems "metastable cavernous systems" (Figure 8). On the other hand, regions of low fracture density, which in our proposed model would be expected to have a lower influx of hydrothermal fluids, may remain less modified by hydrothermal activity, depending on their thickness and compaction, on the amount of water within the deposits, and on the amount/duration of local heat flow.

3.3.1.4. Deconfinement of Pressurized Groundwater Within the Metastable Cavernous Systems

[45] Groundwater emanations to the surface under artesian pressure, or driven by gas exsolution and/or subsurface drainage, may lead to the collapse of the theorized metastable cavernous systems and caprocks, which may result in formation of chaotic terrains, surface depressions, and other tectonic responses to mechanical instability of the plateau regions.

[46] Simple crustal warping and fracturing (Figure 9a) may occur either when collapse occurs to great depths and/or when the collapsing roof is relatively competent and thick compared to the underlying void space. If on the other hand, collapse occurs at shallow depths and/or the thickness of the collapsed region is relatively thin compared to the underlying void space, surface collapse may result in the formation of chaotic terrain [*Komatsu et al.*, 2000] (Figure 9b). Evacuation of collapsed material by floods may produce outflow channels [*Mars Channel Working Group*, 1983].

3.3.1.5. Model Consistency

[47] The model proposed in this section for the formation of metastable cavernous systems filled with pressurized groundwater, and for the evolution of the overlying surface terrain morphologies, is consistent with the occurrence of aligned pits interconnected by troughs within plateau zones modified by surface subsidence and collapse, and adjacent to outflow channels.

[48] The northwestern margin of the pits shown in Figure 7a consist of arcuate ridges, which we interpret as the erosional remnants of geologic materials more competent than both those removed to form the pit, and those forming the highly degraded plateau remnants in the western Aureum Chaos region adjacent to the pit chain.

[49] The higher competence of these ridge-forming materials is consistent with cementation in the periphery of the groundwater-filled cavities, possibly the subsurface zones that surrounded the crater interior deposits such as the interior impact crater walls. Also, in this model the pits are interpreted as formed by surface collapse due to the removal of the interior deposits of buried impact craters. The troughs interconnecting the pits are interpreted as the result of surface collapse over densely packed conduit systems, which formed within overlapping regions of high peripheral interconnectivity of buried impact craters.

[50] *Rodriguez et al.* [2005] show that in some plateau regions in eastern circum-Chryse, the surface terrains have undergone extensive subsidence and fracturing,

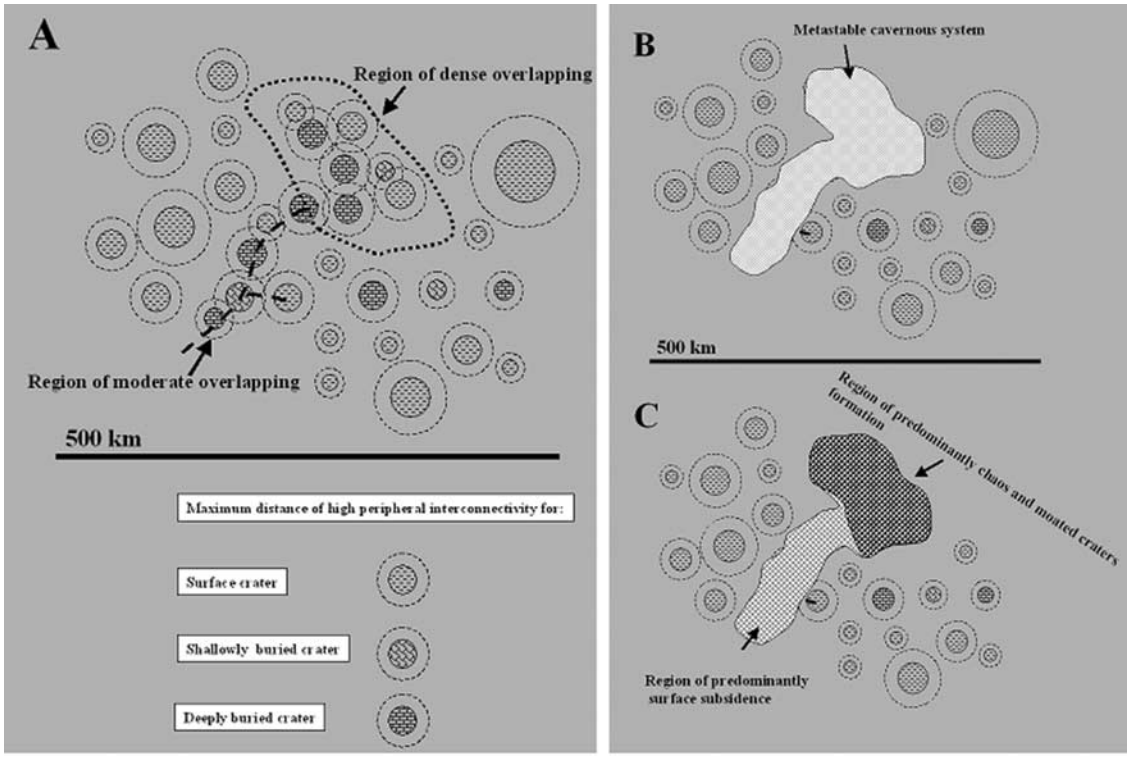

Figure 8. (a) Diagram illustrating the emergence of plateau region high fracture density as a result of both moderate and dense overlapping in the fracture basement associated with each surface and buried randomly distributed impact craters. The dashed circles represent the maximum extent of high peripheral interconnectivity (about 1 crater diameter away from the crater rims), and the patterned circles within represent whether the associated impact craters are in the surface, shallowly buried, or deeply buried (notice that these patterned circles do not represent the diameters of impact craters). (b) Diagram illustrating the transition of the plateau region high fracture density into metastable cavernous systems filled with pressurized groundwater. (c) Groundwater release to the surface (or dissipation in the subsurface) leads to loss of basal support of the cavernous roof and to predominantly surface subsidence in regions of moderate overlapping of the peripheral high interconnectivity regions, and to predominant chaos and moated crater formation in regions of dense overlapping of the high peripheral interconnectivity regions.

subsequently collapsing to shallow depths to form chaotic terrain, where the block distribution is largely nonchaotic, whereas in other plateau regions in eastern circum-Chryse the surface terrains have collapsed to form chaotic terrains where the block distribution is largely chaotic. These geologic scenarios are consistent with the model's prediction that crustal warping and fracturing, or collapse into chaos, may occur depending on the relative thickness of the metastable cavernous systems and the overlying roof materials.

3.3.2. Trends in Surface Subsidence and Collapse in the Plateau Regions Forming the Margins of Chaotic Terrains and Chasmata

[51] The plateau regions forming the margins of the Aureum, Hydraotes, and Hydaspis chaotic terrains show complex linear trends in surface subsidence and collapse, which in this region of eastern circum Chryse has been attributed to the formation of caverns and subsequent collapse of their roof geologic materials, has resulted in systems of elongate valleys, the deepest parts of which tend to form patches of intraplateau chaotic terrains [*Rodriguez et al.*, 2005].

[52] The patterns of surface subsidence indicate that cavernous development occurred in only certain regions of the subsurface of these plateau regions (as opposed to regional chaotic and ''patchy'' subsidence) (e.g., black arrows in Figure 10).

[53] We propose that the observed patterns in subsidence and collapse, in these plateau regions of eastern circum-Chryse, reflect the shape of relatively thick and laterally extensive high fracture density regions, which should be controlled by the interconnection of randomly distributed surface and buried craters that are within range of their respective highly fractured peripheral zones (Figure 8).

[54] Collapse along the zones of surface subsidence has resulted in the formation of pits and arcuate plateau margins, (e.g., black pointers in Figure 10), whose diameters, tend to be between 20 and 40 km, with a maximum depth of $\sim$2 km lower than the surrounding highlands (also see section 3.3.1.1).

[55] Our model indicates that the pits are likely the result of surface collapse over buried impact craters. Arcuate scarps may also result from hillside slumps, especially in fine-grained, saturated sediments. Nevertheless, hillside

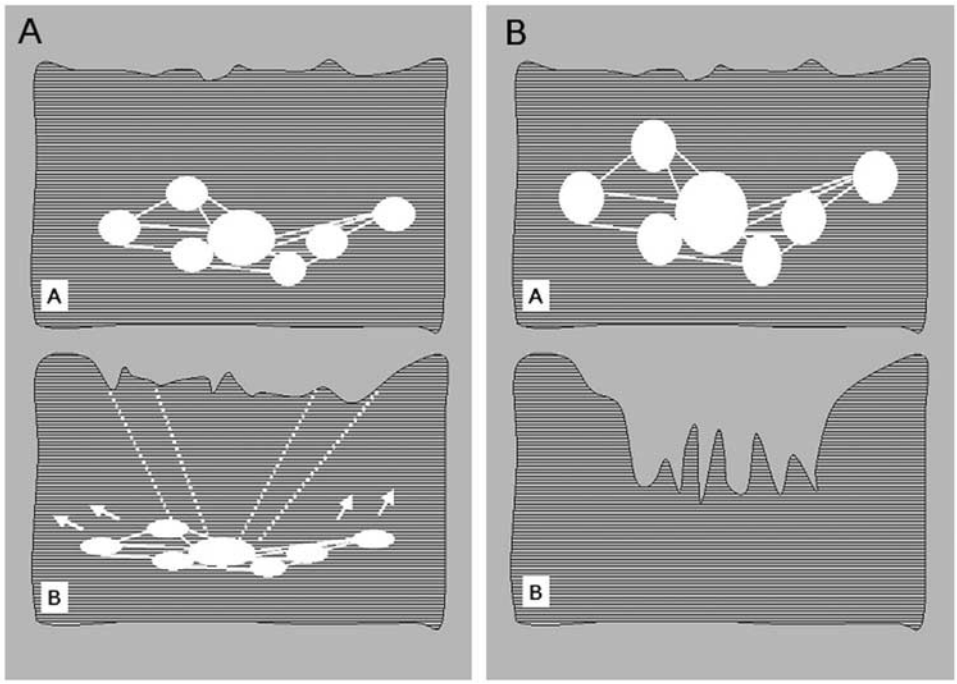

Figure 9. (a) Diagram showing metastable cavernous systems filled with overpressurized water (A) and subsequent collapse of the cavernous region to great depths and/or when the thickness of the roof that collapses is relatively thick when compared to the underlying void space (B). Water is released to the surface by fractures and fault systems (dashed white lines) and/or dispersed into the surrounding porous media (white arrows), which results is surface subsidence such as that observed in the plateau regions north of the Aureum Chaos. (b) Diagram showing metastable cavernous systems filled with overpressurized water (A) and subsequent collapsed of the cavernous region at shallow depths and/or when the thickness of the collapsed region is relatively thin compared to the underlying void space (B). Water is catastrophically released to the surface, and ground collapse results in a chaotic terrain such as that observed in the Aromatum Chaos.

slumping commonly results in significant debris deposits at the foot of the cliff, whereas zones adjacent to truncated impact craters have either less amounts of marginal deposits, or none in some cases.

[56] Although it is difficult to assess the diameter of buried impact craters, our observations indicate that the surface subsidence/collapse and related pit formation, took place primarily by the removal the crater interior deposits, so we propose that the diameter of the collapsed pits may in fact closely represent the diameter of the preexisting buried impact crater. As a consequence, we predict that a significant population of buried impact craters with a diameter range between approximately 20 and 40 km.

[57] On the other hand, there is no significant warping or deformation of the plateau regions forming the margins of the Eos and Ganges chasmata, as well as Valles Marineris to the west (e.g., white arrows in Figure 10). Collapse in the plateau regions along the chasmata forms pits several times deeper and larger than those in the plateau regions around chaotic terrains. For example, the collapse along the margin of the Eos Chasma has, also, resulted in the formation of deep depressions, predominantly about 100 km in diameter and 4 km deeper than the surrounding highland margins (e.g., white pointers in Figure 10), and arcuate cliff margins, which may represent destroyed impact craters.

[58] We propose that collapse and subsidence in the chasmata may have been related to control by east trending macrostructures (defined as tens to thousands of kilometers-long dislocations in the crust [*Dohm et al.*, 2002]) such as faults radial to the Tharsis rise (Figure 10) [e.g., *Tanaka and Golombek*, 1989; *Tanaka et al.*, 1991; *Witbeck et al.*, 1991; *Anderson et al.*, 2001].

[59] We suggest that macrostructures may result in large-scale vertical interconnection along regions of low and high fracture density, thereby interconnecting both systems of dispersed and closely clustered buried impact craters. Deep incision of volatile-enriched materials, coupled with basal warming related to pulses of Tharsis magmatic-driven activity [*Dohm et al.*, 2001], may have resulted in structurally controlled subsurface erosion.

[60] This could account for the absence of plateau warping and subsidence around the collapsed structures in the Eos Chasma and greater depth of collapse. The larger diameters of the collapsed pits (which we interpret as destroyed impact craters), when compared to the diameters those in the plateau regions around the Aureum Chaos, may have resulted from macrostructures interconnecting buried impact craters of various diameters at various depths. The margins of a given collapsed plateau region over metastable cavernous systems (resultant from the interconnection of buried impact craters) would mark the margins of the largest of the buried impact craters in a given region.

[61] We conclude that in eastern circum-Chryse buried impact craters have played a significant role in the subsi-

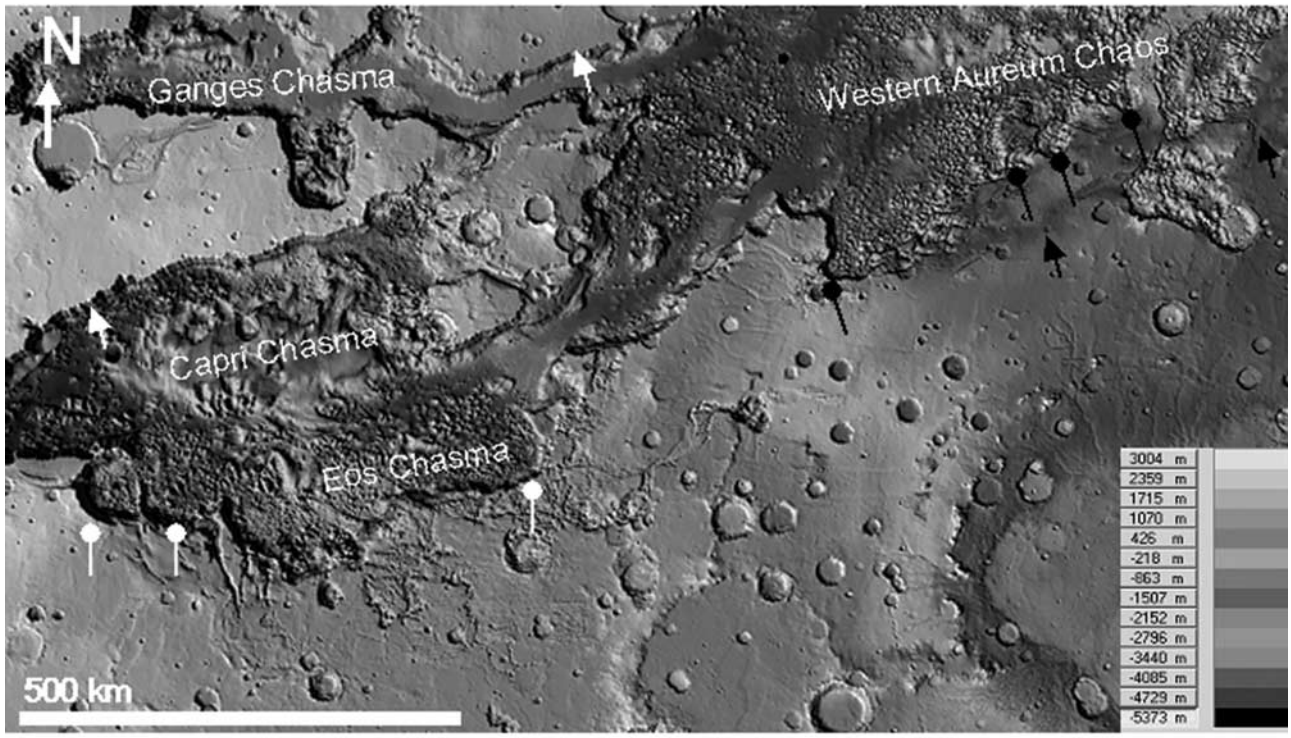

Figure 10. MOLA-derived DEM of the Eos and Capri chasmata and part of the western Aureum Chaos. Region centered at 14.36°S, 318°E. The plateau margins around the chasmata do not show significant warping, which is in contrast with the plateau regions forming the margins around chaotic terrains such as the Aureum Chaos (white and black arrows, respectively). Most of the depressions interpreted as the remnants of impact craters in the collapsed region along the margin of the Eos Chasma (white pointers) are five times larger than those around the margins of the western Aureum Chaos (black pointers) (see Figure 1 for location and context). See color version of this figure in the HTML.

dence and collapse of the plateau regions around both the chasmata and chaotic terrains, as well as in their respective formation. Nevertheless, whereas in the plateau regions of eastern circum-Chryse the distribution of subsurface erosion was controlled by the shape of laterally extensive and thick high fracture density regions, the absence of warping of the plateau margins along the chasmata, and their dominant west trend, suggest that in these regions subsurface erosion was more focused, and possibly controlled by the by fault systems radial to Tharsis.

[62] We propose that structural control by macrostructures on the patterns of ground collapse will increase where basement structures are densely packed (such as in regions proximal to centers of tectonism), or in subsurface regions where buried craters may be relatively dispersed.

[63] Alternative or complementary mechanisms to crater fracture networks, which might result in similar trends of subsidence and collapse, involve (1) the action of multiple mantle plumes, such as shallower micro-plumes resulting from superplume-driven activity (in this way the subsurface would have warmed up locally over a broader region, so that hydrothermal activity and subsurface denudation may then result in both trended and patched subsidence and collapse of surface materials, marking the manifestations of plumes at the Martian surface) [*Dohm et al.*, 2001; *Baker et al.*, 2002; *Komatsu et al.*, 2004], (2) the action of the intrusion of multiple large plutons into the crust [e.g., *Curden et al.*, 2004], or (3) the action of sills/dikes as they flow, as much as thousands of kilometers, along nonisotropic pressure fields related to a main mantle plume [e.g., *Thompson*, 1998].

3.3.3. Formation of Terraced Chaotic Terrains

[64] In a plateau region, mapped by *Rotto and Tanaka* [1995] as the cratered unit of the plateau sequence (Npl1) and the hilly unit (Nplh), there are chaotic terrains, which form systems of terraces, locally marked by channel bedforms (dashed white arrows in Figure 11a). These observations indicate that regional surface collapse has taken place repeatedly and progressively, and that at least some of these episodes of collapse involved the release of large amounts of groundwater.

[65] We propose that the progressive topographic levels of collapsed terrains can be explained by the successive collapse of regions of high fracture density (Figure 11b). The relative thickness of both the regions of high fracture density and regions of low fracture density will determine the number of collapsed plateau levels in a given highland region.

[66] Collapse of outflow channel floor materials (Figure 11c) has also contributed to the formation of the terraced terrains. *Rodriguez et al.* [2005] have proposed that the collapse of outflow channel floor materials may have been related to (1) outflow channel excavation resulting in the injection of pressurized water into porous floor material, and subsequent collapse associated with the

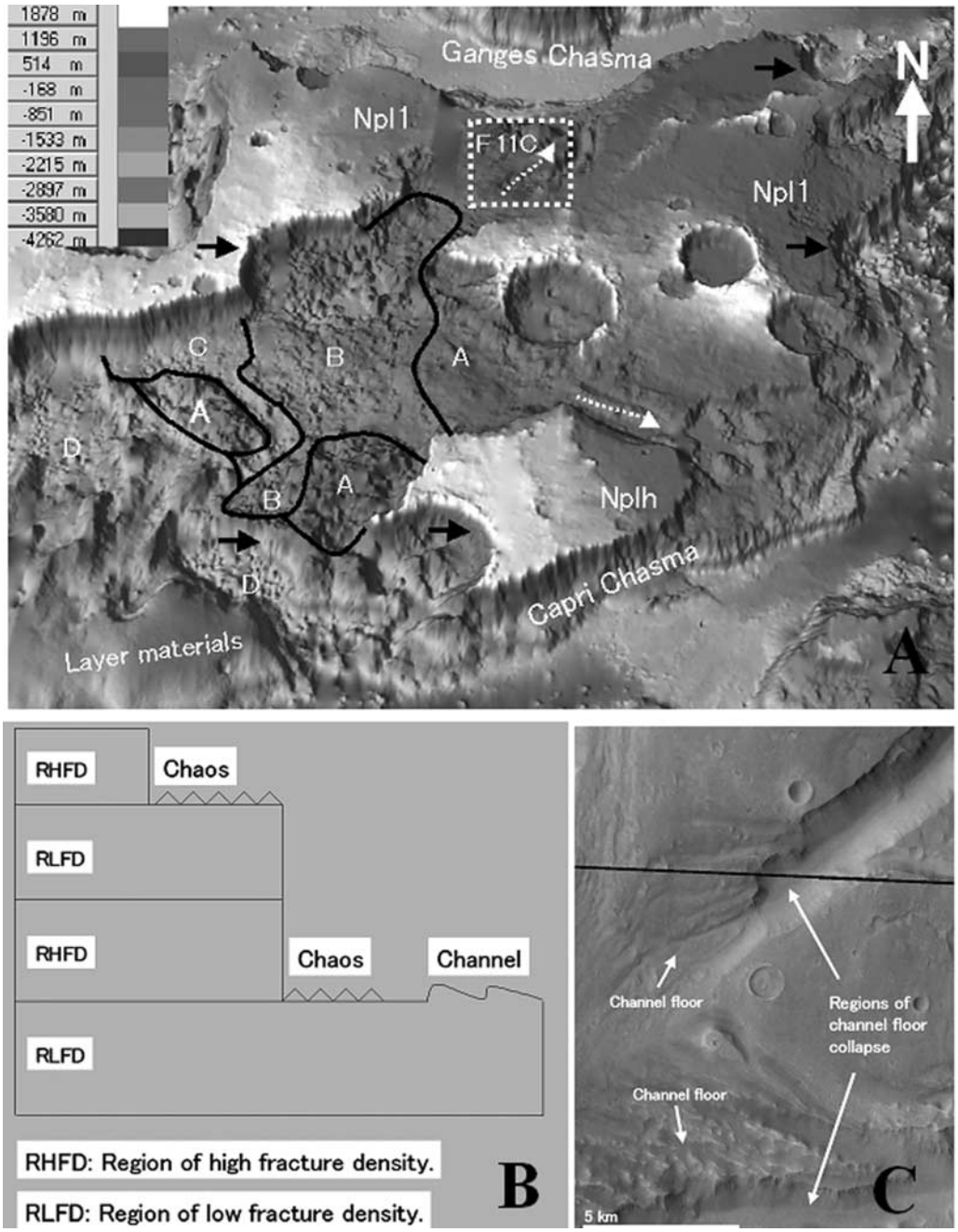

Figure 11. (a) MOLA-based DEM of the Capri Chasma region. Region centered at 14.31°S, 312°E. Image is 350 km wide. Noachian plateau region mapped by *Rotto and Tanaka* [1995] as the cratered unit of the plateau sequence (Npl1) and the hilly unit (Nplh). Letters A to D indicate the topographic levels of chaotic terrains, which form terraces within the plateau. The maximum depth of collapse between the plateau surface and collapse level A is 1500 m, between A and B is 1500 m, between B and C is 1000 m, between C and D is 850 m, and between D and E is 500 m. So the maximum observed thickness of collapsed materials ranges between 1500 and 500 m. In addition, numerous arcuate scarps are visible, interpreted here to be the remains of impact crater walls (black arrows). The white dashed rectangle indicates the location of the region shown in Figure 11c (see Figure 1 for location and context). (b) Diagram illustrating crater fracture networks stratified into regions of relatively thick and laterally extensive high and low fracture density regions. (c) THEMIS V01313002. North azimuth 267.533. Solar azimuth 181.194. Region centered at 9.72°S, 317.00°E. Collapse of outflow channel floor appears to have involved the transition of the dissected terrain into smooth systems of depressions. These relations contrast with those of the Tiu Vallis source region described by *Rodriguez et al.* [2005]; in the Tiu Vallis source region, collapse of channel floors resulted in the formation of blocks and fragmented material (see Figure 11a for location and context).

release of volatiles into the surface and/or atmosphere and/or (2) outflow channel excavation into a deeper cryolithosphere region, resulting in unstable floors subsequent to the exposure of ice-enriched substrates to the atmosphere.

[67] We propose an alternative or complementary hypothesis, which suggests that deposition of wet and warmer sediments onto ice-enriched cold permafrost may have warmed up and increased the ductility of the upper region of the permafrost, which may have led to instability and collapse and/or subsidence of the outflow channel floor.

[68] Numerous arcuate scarps, which are visible in Figure 11a (black arrows), are interpreted here to be truncated impact craters. These truncated impact craters are preferentially preserved at distinct broad terraced surfaces (topographic levels of subsidence) and form the margins of the deepest regions within each of the terraces. Moreover, collapse features are more prominent on the floors of impact craters (when compared to the surrounding plateau material (see section 3.3.4)). These observations are consistent with our hypothesis, which proposes that hydrothermal activity within regions of high fracture density is greater within crater interior deposits and results in the preferential removal of subsurface materials.

[69] Our interpretations hint at the formation of, at least part of the Capri Chasma by progressive collapse of the highland, which indicates that in these plateau regions the crater fracture networks consist predominantly of alternating, relatively thin and laterally extensive, high and low fracture density regions. Therefore the greater depth of collapse observed in these chasmata regions can be explained by the interconnection of these regions by macrostructures and their subsequent progressive collapse (see sections 3.3.2 and 3.3.4).

[70] This proposition has important implications for the hydrologic history of the region. For example, catastrophic collapse of the plateau regions to the present floor of the Capri and Ganges chasmata would have dissipated vast amounts of energy and possibly resulted in the release of very large amounts of groundwater and other fluidized materials.

3.3.4. Formation of Craters With Moats in Eastern Circum-Chryse Region

[71] In the circum-Chryse region, fractured crater floors predominantly develop in Noachian plateau terrains east of Valles Marineris, where *Rodriguez et al.* [2005] have proposed that cavernous collapse led to surface subsidence and breakup of plateau materials into chaos (Figure 12). These fractured floors often form moats which surround plateaus and contain broken material (Figure 12a), marking the location of a highly degraded impact crater rims and crater interior deposits (Figure 13a). Moats occur in impact craters of varying diameters and relative ages. In this section

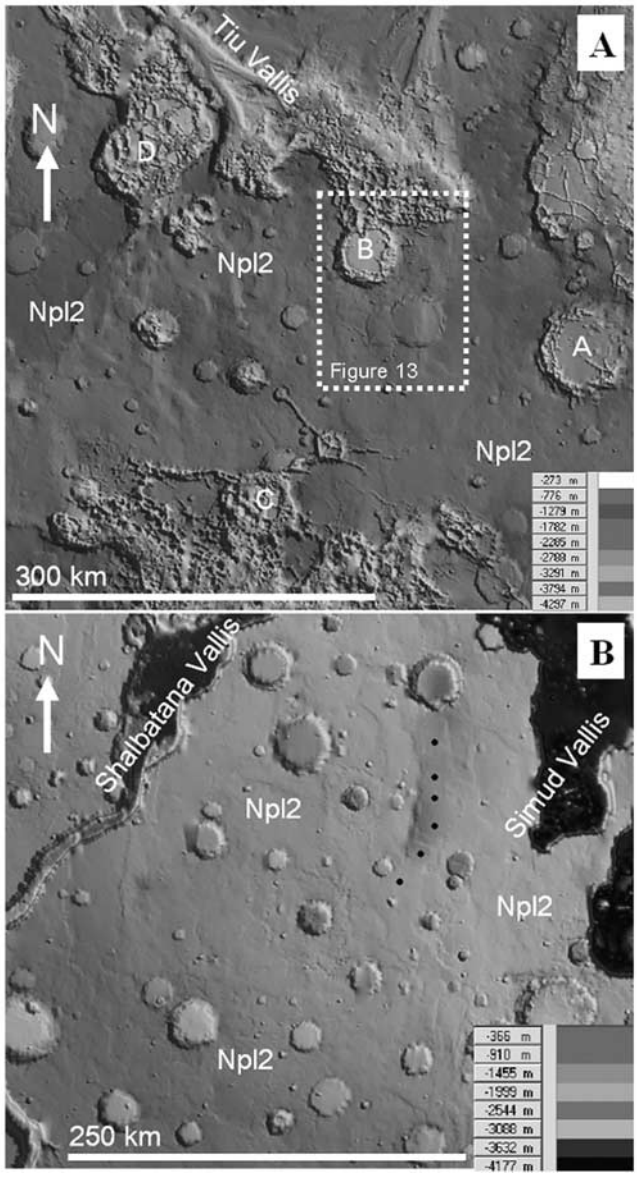

Figure 12. (a) MOLA-based DEM of a region forming part of the Late Noachian subdued crater unit (Unit Npl_2) of the plateau sequence [*Scott and Tanaka*, 1986; *Rotto and Tanaka*, 1995] north of the Aureum Chaos and west of the Hydraotes Chaos. Region centered at 0.42°N, 333.50°E. Illumination from the southwest. *Rotto and Tanaka* [1995] described this map unit as smooth to undulatory intercrater plains with partly buried, mostly rimless and flat-floored impact craters. *Rodriguez et al.* [2005] mapped this region of the Nlp2 as the subsided plateau region, which they propose to have undergone extensive subsidence of plateau materials over subterranean cavernous systems. Many impact craters within the subsided plateau region develop moats (e.g., A-D), which is consistent with a genetic linkage among basement structural fabric (including buried impact craters and associated structures and regional fault systems) and the processes that result in ground subsidence and the formation of moated craters (see Figure 1 for location and context). (b) MOLA-based DEM of another region forming part of the Late Noachian subdued crater unit (Unit Npl_2) of the plateau sequence [*Scott and Tanaka*, 1986; *Rotto and Tanaka*, 1995] west of the Simud Vallis. Region centered at 5.68°N, 320.32°E. Illumination from the southwest. In contrast to the subsided plateau regions [*Rodriguez et al.*, 2005], craters in this region do not tend to have moats. The sequence of black dots indicates an elongate depression, which could have resulted from surface subsidence over cavernous systems (see Figure 1 for location and context).

we discuss mechanisms to explain both the formation of moats, as well as their preferential occurrence in plateau regions apparently modified by cavernous collapse.

[72] Moats appear to be restricted to the margins of highly degraded crater rims (Figure 12). The broken terrain within moats comprises isolated and coalescing knobs, which form ridges concentric to the central part of the impact crater (Figure 13a). Also, radial and concentric troughs about the impact crater (Figure 13a) form to a distance of about 1/3 of the crater diameter from the crater rim, which is consistent with the proposed range of distance of high peripheral interconnectivity described in section 3.2.2.

[73] These observations suggest that interconnected concentric and radial faults are more densely packed around the periphery of impact craters. This could be related to the fact that during the early modification stage of impact crater formation concentric faults may form during both the inward collapse of the crater wall, as well as the outward collapse of the central uplift [*Osinski and Spray*, 2003]. Peripheral fault systems may have also been produced after the formation of impact craters by processes such as the injection of tabular magmatic localized underneath their floors and associated uplift [*Schultz and Glicken*, 1979].

[74] *Rodriguez et al.* [2005] have proposed that lobate features observed on the central fractured plateau region of crater (C-A) in Figure 13a were deposited by fracture-fed fluids, indicating the existence of large subsurface liquid reservoirs and the upward migration of pressurized groundwater.

[75] The region beneath the floors of some impact craters consists of a mixture of breccias and impact melt (e.g., *Spray et al.* [2004] show that under the 130 km in diameter Sudbury crater in Ontario, Canada, there is a melt sheet ~2.5 km thick underneath the Onaping Formation, a 1 km thick fallback breccia). If there is a high amount of melt and/or a high degree of cementation by mineral precipitation related to hydrothermal activity [*Newsom et al.*, 1996], then this region is likely to have lower permeability and be more competent than the densely fractured and more friable impact crater peripheral regions.

[76] We propose that hydrologic activity around the periphery of impact craters will be enhanced due to the relatively higher permeability and relatively lower competence of geologic materials forming this region, resulting from the dense packing of extensional faults. As a consequence, subsurface erosion localized around the periphery of impact crater may have led to the formation of moats.

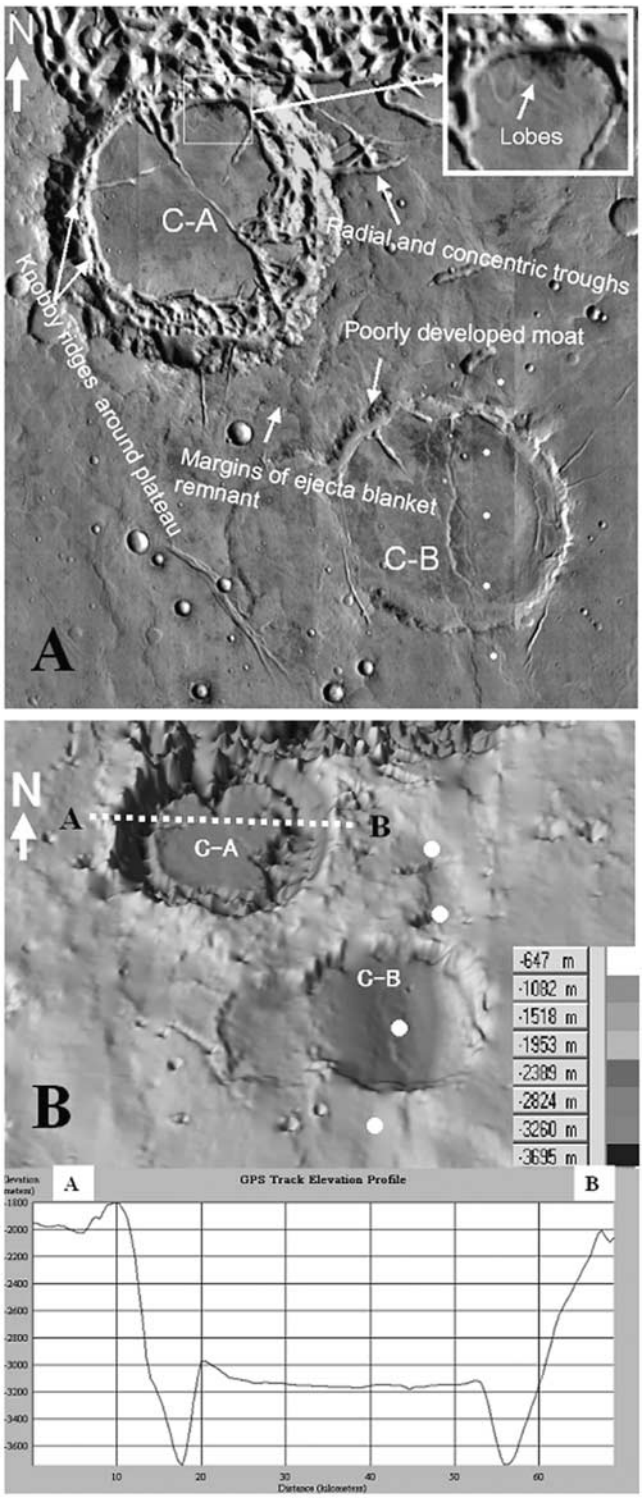

Figure 13. (a) THEMIS day infrared composite. Region centered at 0.68°N, 334.69°E. A 50-km-diameter impact crater (C-A) has a collapsed floor, which forms a moat around a central plateau near the western margin of the Hydaspis Chaos. Remnants of an ejecta blanket can be traced around the impact crater, except where destroyed by the development of chaotic terrain to the north. On the other hand, another impact crater in the region (C-B) has no discernable ejecta materials, indicating an older age when compared to C-A. There is a north trending depression (white dots) that transects the subsided plateau region and is most distinct on the floor of C-B. A trough, which locally encircles the central part of C-B (white pointers), may represent a poorly developed moat (see Figure 12 for location and context). (b) MOLA-based DEM. Region centered at 0.68°N, 334.69°E. Crater (C-A) is 50 km in diameter. The white dots indicate the central part of a north trending depression shown in Figure 13a. The elongate depression is 30 km wide and 300 m deep. The MOLA elevation profile (A to B) clearly shows the moat in the crater.

[77] Undermining and disintegration of crust near the base of interior layered crater-fill deposits and ice-filled fractured zones beneath individual buried impact craters might cause warping, sagging, and fracturing of the layered deposits. Similarly, radial and concentric regions of high fracture density and crater fracture networks may undergo hydrothermal advection, ice destabilization at depth, and collapse of frozen permafrost near the surface.

[78] Different degrees of moat formation (Figure 12a) may be related to either progressive degradational processes, or to variability in the intensity and/or duration of the degradational processes. The fact that the surface collapse that led to the formations of moats did not result in chaotically distributed broken up plateau materials suggests that the energy dissipated during collapse was not high enough as to destroy the local tectonic fabrics by the turbulent disintegration of the geologic column, so that the mode of collapse was not catastrophic.

[79] *Schultz and Glicken* [1979] proposed that modification processes are localized by the impact structures and restricted to the crater interiors. They interpret this to be the result of heat generated by a tabular magmatic intrusion injected beneath the brecciated zone of an impact crater, which raises the temperature of the overlying material. Thawed materials would then subsequently escape through the peripheral fracture system surrounding the crater, or alternatively, a metastable state of liquefaction could occur, if the material is confined or the rate of thawing exceeds the rate of escape.

[80] We propose that the impact craters modified by moats in eastern circum-Chryse primarily occur in the upper zones of relatively thick and laterally extensive high fracture density regions, particularly where there is dense overlapping of the peripheral high interconnectivity regions (Figure 8). The formation of moats would have been related to nonuniform heat flow controlled by the shape of these high fracture density regions so that hydrothermal activity, and associated subsurface erosion, would affect only the surface/shallowly buried impact crater that formed part of a certain high fracture density region (Figure 14).

[81] *Rodriguez et al.* [2005] note that the Hydaspis Chaos mainly comprises a cluster of collapsed craters, which is consistent with preferential deconfinement and emanations of pressurized and fluidized volatile-enriched materials within craters forming part of metastable cavernous systems.

[82] Our views indicate that the processes responsible for the formation and distribution of moated craters were controlled by regional basal structures (high fracture density regions). This is contrast with previous interpretations, which suggest that the formation and distribution of moated craters was related to tabular intrusions being injected under crater floors and/or to processes exclusively controlled by structures localized within impact craters [*Schultz and Glicken*, 1979].

[83] The model presented here is able to readily explain the following:

[84] 1. Moated craters are clustered in plateau regions apparently modified by cavernous collapse, and moats develop only in certain craters for a given region (Figures 12a, 13, and 14).

[85] 2. Moat formation affects impact craters of varying diameters and relative ages.

[86] 3. The formation of the moat shown in Figure 13 suggests large-scale removal of geologic materials, which can be easily explained by subsurface erosion related to that hydrologic activity within extensive and highly interconnected subsurface hydrologic systems such as the hypothesized metastable cavernous systems.

4. Discussion

[87] The hypotheses proposed in this work consist of geologic scenarios related to the existence of impact crater fracture networks within the Martian icy cryolithospheric regions. In these geologic scenarios we have tried to explain assemblages of warped and collapsed landforms observed in plateau regions of eastern circum-Chryse. In the following discussion we will briefly address implications of crater fracture networks for the paleohydrologic and volcanic evolutions of Mars, as well as for astrobiology and human exploration.

4.1. Progressive Aquifer Depletion Versus Punctual Mechanical Instability of Groundwater

[88] We propose that progressively smaller floods may not necessarily reflect depletion of regional aquifer systems. An alternative, or complementary, view to this hypothesis is that through time, progressively smaller volumes of subterranean water systems became mechanically unstable, resulting in progressively smaller floods. This scenario may have resulted if there were progressively smaller intrusive magmatic events and/or if the regions of study were predominantly affected by only certain magmatic episodes.

[89] In these regions, we suggest that regions of high fracture density may still be stable and so represent regions of high water concentration within the Martian upper crust. These regions may be frozen, or still partly liquid if brine composition and heat flow allows.

4.2. Effusive Volcanism From Distal Magma Chamber

[90] Convergence of dikes into cavernous systems and/or cavities may take place depending on the geometric characteristics, distribution, density, and proximity of the putative subterranean systems (A. Rubin, personal communication, 2004). We propose that if dikes converge into caverns or cavities, secondary magma chambers may form. Magmatic differentiation may result in a buoyant magma phase, which may use dense fracture systems as conduits to erupt onto the surface, forming fissure-fed lava systems (e.g., dispersed venting). This hypothesis may help explain how lava flow fields commonly occur in the absence of volcanic constructs (e.g., centralized venting).

4.3. Astrobiological and Human Exploration

[91] Subterranean cavernous environments in the Tharsis and surrounding regions, where liquid water and relatively warm conditions, may have been stable for long periods of time, and where episodic magmatism provided energy and nutrients to the subterranean environments, are considered here to represent prime sites for future astrobiological investigation.

[92] For example, some cavernous environments have been exposed to the atmosphere through collapse, such as reported for Aureum Chaos [*Rodriguez et al.*, 2005],

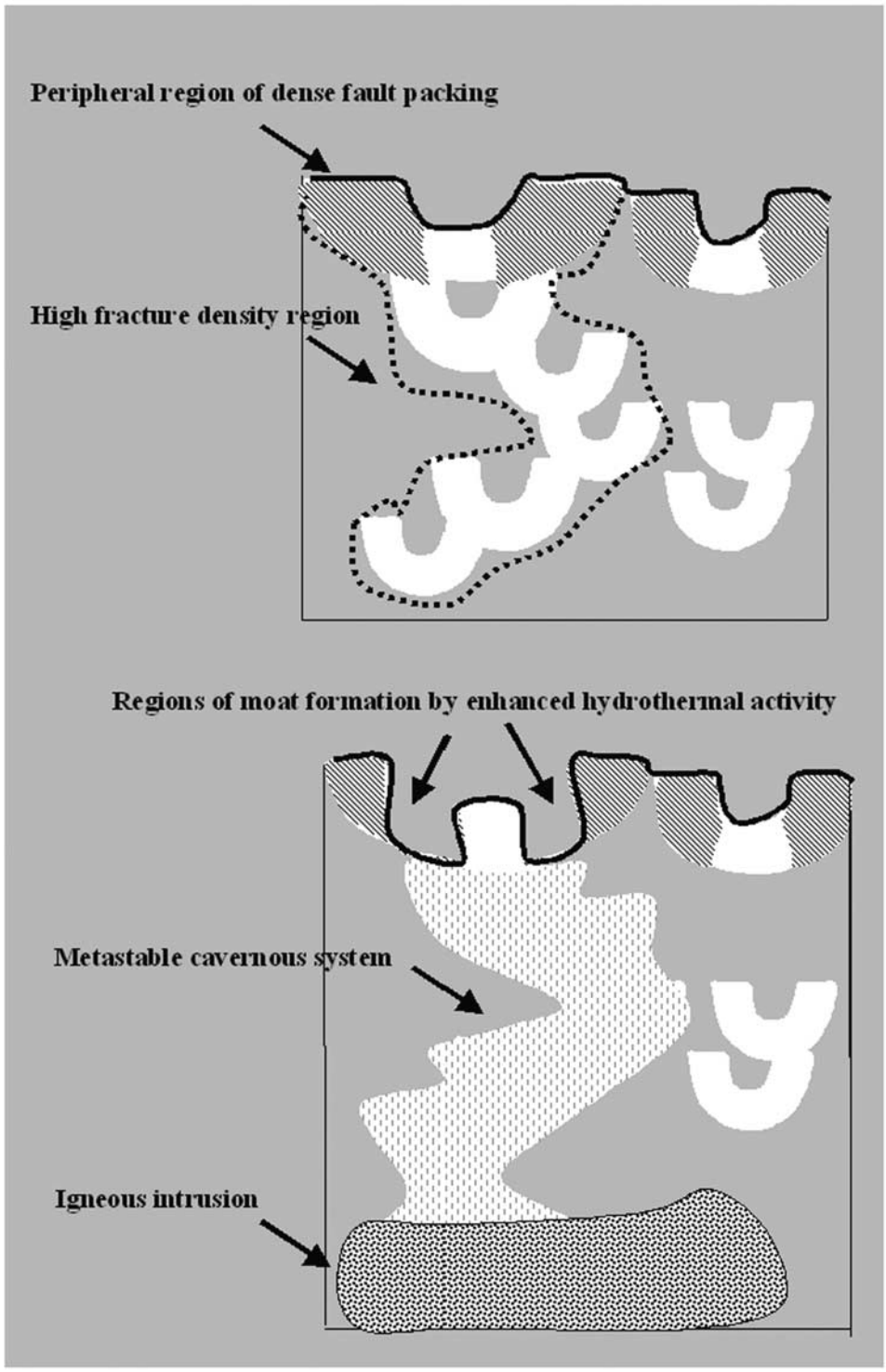

Figure 14. Diagram illustrating a thick region of high fracture density, which extends all the way up to the surface (black dotted line) (top). An igneous intrusion (bottom) results in the transition of the high fracture density region into a metastable cavernous system. Associated hydrothermal plumes erode the periphery of the impact crater forming the top of the high fracture density region, resulting in surface collapse and the formation of a moat. Notice how an adjacent impact crater, which does not form part of the high fracture density region, is not modified.

making potential records of possible extant (e.g., fluid inclusions) and fossilized life accessible at the surface. Another example is the plateau region forming the northern margin of the Ganges Chasma (Figure 15), considered a type locality for the proposed hypotheses presented here.

[93] In this region, there are diverse systems of long depressions along which there are pit chains. It is generally

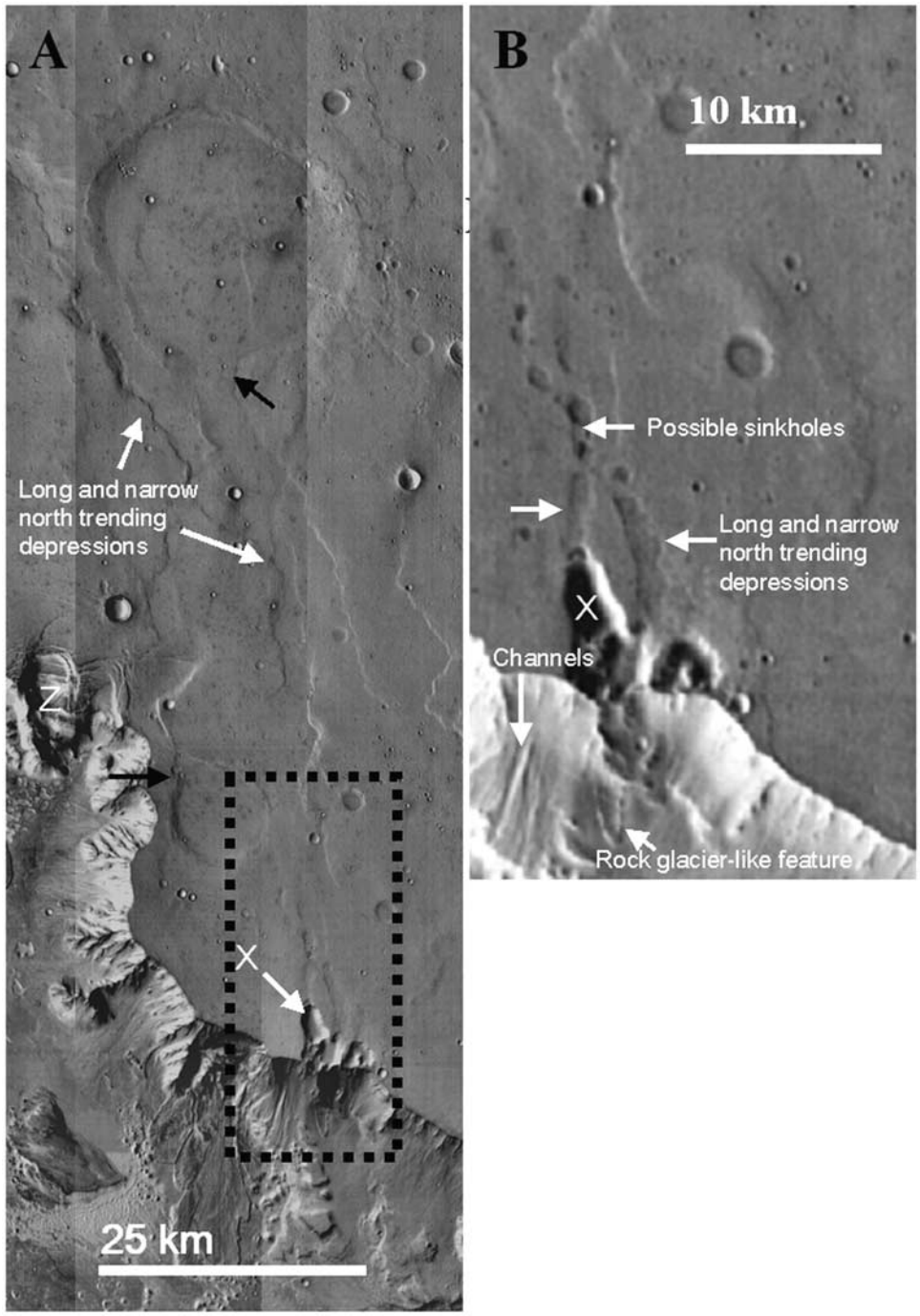

Figure 15. (a) THEMIS day infrared composite. Region centered at 5.97°S, 314.13°E. The plateau region forming the northern margin of the Ganges Chasma is dissected by interconnected and predominantly north trending, elongated depressions (white arrows). Some of these depressions terminate in enclosed collapsed regions (Z) and in regions where the plateau surface has apparently collapsed (X). Elongated depressions transect two quasi-circular depressions (black arrows), which resemble buried impact craters, appearing to lower the crater margins (see Figure 1 for location and context). (b) THEMIS day infrared composite. Region centered at 5.97°S, 314.13°E. Close-up of feature X. The putative collapsed region X forms the southern part of a north trending chain of depressions (white arrows), some of which appear to be sinkholes (see Figure 15a for location and context).

agreed that pit chains are formed by collapse into a subsurface cavity or by explosive eruption [*Tanaka and Golombek*, 1989; *Spencer and Fanale*, 1990; *Davis et al.*, 1995; *Mège and Masson*, 1996, 1997; *Tanaka*, 1997; *Liu and Wilson*, 1998; *Mège*, 1999; *Montesi*, 1999; *Scott et al.*, 2000; *Gibbons et al.*, 2001; *Mège et al.*, 2000, 2002, 2003; *Scott and Wilson*, 2002; *Wilson and Head*, 2002; *Ferrill et al.*, 2003; *Wyrick et al.*, 2003].

[94] On the basis of pit morphology, volume calculations, structural associations (e.g., normal faults, grabens), vertical offset of pits and general lack of associated volcanic features, *Wyrick et al.* [2004] indicate that most pit chains in the western hemisphere of Mars form over dilational normal faults or extension fractures. Nevertheless, the association of pits with regions of extensive surface subsidence and collapse (e.g., in the Shalbatana channel source region described by *Rodriguez et al.* [2003] and white arrows in Figure 15) favors the hypothesis that, at least in eastern circum-Chryse, the formation of pit chains may mark deformation associated with subsidence of overlying materials into complex cavernous systems.

[95] Localized collapse of the surface over cavernous regions (X and Z in Figure 15) may have resulted in emanations of ancient water brines, as indicated by the presence of channels and rock glacier-like feature close to the putative collapse region X in Figure 15b. Exposed subsurface geologic materials, as well as materials deposited by local water emanations, should comprise prime sites for astrobiological exploration in future missions, since they offer windows into Martian subsurface environments, where life may have been stable over long geologic timescales. Moreover, these sites are significantly more accessible than those developed in chaotic terrains.

[96] Our observations of this region indicate the existence of relatively stable subterranean cavernous systems when compared to other areas that exhibit more complex broken terrain.

5. Conclusions

[97] Our study of the hydrogeologic and structural roles of buried and surface impact crater populations on Mars permits the following conclusions to be drawn:

[98] 1. The upper Martian crust is not structurally similar to that of the moon, composed primarily of fractured primordial basement rocks and an overlying impact-generated megaregolith. Instead much of the "pre-Noachian" basement and plateau materials were deposited in ancient paleobasins, prior to reworking during the heavy bombardment into the Early Noachian and later surfaces.

[99] 2. There are large populations of buried impact craters on Mars.

[100] 3. Many of the Noachian (and "pre-Noachian") buried impact craters are likely to contain H_2O-enriched infilling materials.

[101] 4. Intermingling concentric and radial fracture systems associated with multiple surface and/or buried impact craters will have resulted in complex impact crater fracture networks in uncompacted plateau and plains geologic materials.

[102] 5. Impact crater fracture networks associated with closely clustered populations of surface and/or buried impact craters will form high fracture density region. On the other hand, impact crater fracture networks associated with sparsely spaced populations of surface and/or buried impact craters will produce low fracture density regions.

[103] 6. The configurations of high and low fracture density subsurface zones for a given uncompacted subsurface zone may include (1) relatively thick and laterally extensive high fracture density regions and/or (2) alternating, relatively thin and laterally extensive, high and low fracture density regions.

[104] 7. If during a given episode of high heat flow, meltwater was produced or groundwater was stable within the subsurface. Control of hydrothermal circulation by the faults radiating from individual craters within regions of high fracture density, would imply that heat flow will tend to converge into the base of the impact H_2O-enriched infilling materials. Removal of crater geologic materials and segregation of the liquid water phase may result in the formation of extensive and confined water-filled caverns in some regions of high fracture density within water-enriched zones of the Martian cryolithosphere.

[105] 8. The transient balance between the hydrostatic pressure exerted by the confined groundwater and the lithostatic pressure exerted by the confining geologic materials may result in these caverns being highly unstable. On Mars, cavernous collapse may have resulted in surface subsidence or breakup of plateau materials into diverse types of chaotic terrains (including terraced chaos moated craters). Release of pressurized groundwater may have resulted in extensive fluvial activity.

6. Unresolved Issues and Future Work

[106] Since regional plateau subsidence generally is concurrent or postdates outflow activity in the Hydaspis Chaos [*Rodriguez et al.*, 2005], by knowing the age of outflow channel formation, the timing of ground subsidence may be estimated, and thus the timing of basal warming. Key unresolved issues include duration of (1) the metastable stage in subterranean cavernous systems, (2) stage of plateau extensional warping, and (3) breakdown of plateau materials into chaotic terrain.

[107] On Mars, where impact crater fracture networks significantly influenced geologic and hydrogeologic systems, so, too, is this expected for other terrestrial planets, and for the early Earth. In particular, the role of impact-related fracture networks on the possible distribution of subsurface water on the Moon and Mercury, if we consider permanently shadowed craters in the polar regions to be water capture zones.

[108] **Acknowledgments.** The authors would like to thank Robert C. Anderson and Jens Ormö for their insightful reviews. We also thank Devon M. Burr, who acted as an internal USGS reviewer and whose comments and suggestions substantially improved this work. Thanks also to Jorge Hernandez Rodriguez, who provided technical assistance in the elaboration of some of the computer-generated illustrations. We give credit to Philip Christensen, at Arizona State University, for the elaboration of the THEMIS data release Web site (http://themis.asu.edu/), which we have extensively used during the research that led to the completion of this work. We would also like to thank Lionel Wilson for his comments and suggestions, which considerably improved this paper.

References

Abineri, K. W. (1995), The western floor of the lunar formation Schickard, *J. Br. Astron. Assoc.*, *105*(6), 301–307.

Anderson, R. C., J. M. Dohm, M. P. Golombek, A. F. C. Haldemann, B. J. Franklin, K. L. Tanaka, J. Lias, and B. Peer (2001), Primary centers and secondary concentrations of tectonic activity through time in the western hemisphere of Mars, *J. Geophys. Res.*, *106*(E9), 20,563–20,586.

Baker, V. R. (2001), Water and the Martian landscape, *Nature*, *412*, 228–236.

Baker, V. R., R. G. Strom, V. C. Gulick, J. S. Kargel, G. Komatsu, and V. S. Kale (1991), Ancient oceans, ice sheets and the hydrological cycle on Mars, *Nature*, *352*, 589–594.

Baker, V. R., R. G. Strom, J. M. Dohm, V. C. Gulick, J. S. Kargel, G. Komatsu, G. G. Ori, and J. W. Rice (2000), Mars' Oceanus Borealis, ancient glaciers, and the MEGAOUTFLO hypothesis, *Proc. Lunar Planet. Sci. Conf. 31st*, abstract 1863.

Baker, V. R., S. Maruyama, and J. M. Dohm (2002), A theory of early plate tectonics and subsequent long-term superplume activity on Mars, *Electron. Geosci.*, *7*. (Available at http://192.129.24.144/licensed_materials/10069/free/conferen/superplu/index.html)

Banerdt, W. B., M. P. Golombek, and K. L. Tanaka (1992), Stress and tectonics on Mars, in *Mars*, edited by H. H. Kieffer et al., pp. 249–297, Univ. of Ariz. Press, Tucson.

Boston, P. J., et al. (2001), Cave biosignature suites: Microbes, minerals and Mars, *Astrobiology*, *1*, 25–56.

Boynton, W. V., et al. (2002), Distribution of hydrogen in the near surface of Mars: Evidence for subsurface ice deposits, *Science*, *297*, 81–85.

Carr, M. H. (1979), Formation of Martian flood features by release of water from confined aquifers, *J. Geophys. Res.*, *84*, 2995–3007.

Carr, M. H. (1996), *Water on Mars*, Oxford Univ. Press, New York.

Carr, M. H. (2002), Elevations of water-worn features on Mars: Implications for circulation of groundwater, *J. Geophys. Res.*, *107*(E12), 5131, doi:10.1029/2002JE001845.

Chapman, M. G., and K. L. Tanaka (2002), Related magma-ice interactions: Possible origins of chasmata, chaos and surface materials in Xanthe, Margaritifer, and Meridiani Terrae, Mars, *Icarus*, *155*, 324–339.

Clifford, S. M. (1993), A model for the hydrologic and climatic behavior of water on Mars, *J. Geophys. Res.*, *98*, 10,973–11,016.

Clifford, S. M., and T. J. Parker (2001), The evolution of the Martian hydrosphere: Implications for the fate of a primordial ocean and the current state of the northern plains, *Icarus*, *154*, 40–79.

Cohen, J. L., and A. H. Treiman (1999), The longitudinal extent of a layered sequence in the sub-surface of Mars: Evidence for diagenesis in the Hesperian, *Proc. Lunar Planet. Sci. Conf. 30th*, abstract 1254.

Craddock, R. A., and T. A. Maxwell (1993), Geomorphic evolution of the Martian highlands through ancient fluvial processes, *J. Geophys. Res.*, *98*, 3453–3468.

Curden, A. R., A. Carlos, D. D. Davis, and J. Grocott (2004), Timescales and mechanisms of batholith construction, Costal Cordillera, Northern Chile, from precise U-Pb zircon ages and regional geochronological data, *Eos Trans. AGU*, *85*(47), Fall Meet. Suppl., Abstract V52B-02.

Davis, P. A., K. L. Tanaka, and M. P. Golombek (1995), Topography of closed depressions, scarps, and grabens in the North Tharsis Region of Mars: Implications for shallow crustal discontinuities and graben formation, *Icarus*, *114*, 403–422.

Dohm, J. M., J. C. Ferris, V. R. Baker, R. C. Anderson, T. M. Hare, R. G. Strom, N. G. Barlow, K. L. Tanaka, J. E. Klemaszewski, and D. H. Scott (2001), Ancient drainage basin of the Tharsis region, Mars: Potential source for outflow channel systems and putative oceans or paleolakes, *J. Geophys. Res.*, *106*, 32,943–32,958.

Dohm, J. M., S. Maruyama, V. R. Baker, R. C. Anderson, J. C. Ferris, and T. M. Hare (2002), Plate tectonism on early Mars: Diverse geological and geophysical evidence, *Proc. Lunar Planet. Sci. Conf. 33rd*, abstract 1639.

Dohm, J. M., et al. (2004), Ancient giant basin/aquifer system in the Arabia region, Mars, and its influence on the evolution of the highland-lowland boundary (abstract), paper presented at Workshop on Hemispheres Apart: The Origin and Modification of the Martian Crustal Dichotomy, Lunar and Planet. Inst., Houston, Tex.

Fairén, A. G., and J. M. Dohm (2004), Age and origin of the lowlands of Mars, *Icarus*, *168*, 277–284.

Fairén, A. G., J. Ruiz, and F. Anguita (2002), An origin for the linear magnetic anomalies on Mars through accretion of terranes: Implications for dynamo timing, *Icarus*, *160*, 220–223.

Fairén, A. G., J. M. Dohm, V. R. Baker, M. A. de Pablo, J. Ruiz, J. Ferris, and R. C. Anderson (2003), Episodic flood inundations of the northern plains of Mars, *Icarus*, *165*, 53–67.

Ferrill, D. A., and A. P. Morris (2003), Dilational normal faults, *J. Struct. Geol.*, *25*, 183–196.

Ferrill, D. A., A. P. Morris, D. J. Waiting, N. M. Franklin, and D. W. Sims (2003), Influence of gravity on the geometry of Martian normal faults, *Proc. Lunar Planet. Sci. Conf. 24th*, abstract 2050.

Frey, H. V. (2004), A timescale for major events in early Mars crustal evolution, *Proc. Lunar Planet. Sci. Conf. 35th*, abstract 1382.

Fuks, K. H., A. H. Treiman, and S. Murchie (1995), Layering in the upper walls of Valles Marineris, Mars: A diagenetic origin (abstract), *Proc. Lunar Planet. Sci. Conf. 36th*, 431.

Garvin, J. B., S. E. H. Sakimoto, J. J. Frawley, and C. Schnetzler (2000), North polar region crater forms on Mars: Geometric characteristics from the Mars Orbiter Laser Altimeter, *Icarus*, *144*, 329–352.

Gibbons, H. L., E. D. Scott, L. Wilson, and J. W. Head (2001), Inferred properties of giant radial dikes beneath graben in Northern Tharsis, Mars, *Proc. Lunar Planet. Sci. Conf. 32nd*, abstract 1154.

Gurov, E. P., and E. P. Gurova (1982), Some regularities in the areal spreading of fractures around Elgygytgyn crater (abstract), *Proc. Lunar Planet. Sci. Conf. 13th*, Part 1, *J. Geophys. Res.*, *87*, suppl., A291–A292.

Horstman, K. C., and H. J. Melosh (1989), Drainage pits in cohesionless materials: Implications for the surface of PHOBOS, *J. Geophys. Res.*, *94*, 12,433–12,441.

Hynek, B. M., R. J. Phillips, and R. E. Arvidson (2003), Explosive volcanism in the Tharsis region: Global evidence in the Martian geologic record, *J. Geophys. Res.*, *108*(E9), 5111, doi:10.1029/2003JE002062.

Kling, G. W., W. C. Evans, M. L. Tuttle, and G. Tanyileke (1994), Degassing of Lake Nyos, *Nature*, *368*, 405–406.

Komatsu, G., J. S. Kargel, V. R. Baker, R. G. Strom, G. G. Ori, C. Mosangini, and K. L. Tanaka (2000), A chaotic terrain formation hypothesis: Explosive outgas and outflow by dissociation of clathrate on Mars (abstract), *Proc. Lunar Planet. Sci. Conf. 31st*, 1434.

Komatsu, G., J. M. Dohm, and T. M. Hare (2004), Hydrogeologic processes of large-scale tectono-magmatic complexes in Mongolia-southern Siberia and on Mars, *Geology*, *32*, 325–328.

Kuzmin, R. O., and E. V. Zabalueva (1998), On salt solutions in the Martian cryosphere, *Sol. Syst. Res.*, *32*(3), 187–197.

Liu, S. Y., and L. Wilson (1998), Collapse pits due to gas release from shallow dikes on Mars, *Proc. Lunar Planet. Sci. Conf. 29th*, abstract 1602.

Mader, H. M., Y. Zhang, J. C. Phillips, R. S. J. Sparks, B. Sturtevant, and E. M. Stolper (1994), Experimental simulations of explosive degassing of magma, *Nature*, *372*, 85–88.

Malin, M. C., and K. S. Edgett (1999), An emergent, new paradigm for Mars geology, paper presented at Fifth International Conference on Mars, Calif. Technol. Inst., Pasadena, Calif.

Malin, M. C., and K. S. Edgett (2000), Sedimentary rocks of early Mars, *Science*, *290*(5498), 1927–1937.

Mars Channel Working Group (1983), Channels and valleys on Mars, *Geol. Soc. Am. Bull.*, *94*, 1035–1054.

Max, M. D., and S. M. Clifford (2000), The state, potential distribution, and biological implications of methane in the Martian crust, *J. Geophys. Res.*, *105*, 4165–4171.

McKenzie, D., and F. Nimmo (1999), The generation of Martian floods by the melting of ground ice above dykes, *Nature*, *397*, 231–233.

Mège, D. (1999), Graben morphology, dike emplacement, and tension fracturing in the Tharsis igneous province of Mars (abstract), paper presented at Fifth International Conference on Mars, Calif. Technol. Inst., Pasadena, Calif.

Mège, D., and P. Masson (1996), A plume tectonics model for the Tharsis province, Mars, *Planet. Space Sci.*, *44*(12), 1499–1546.

Mège, D., and P. Masson (1997), Graben formation and dike emplacement on Earth and other planets, *Proc. Lunar Planet. Sci. Conf. 28th*, abstract 1229.

Mège, D., Y. Lagabrielle, E. Garel, M. H. Cormier, and A. C. Cook (2000), Collapse features and narrow grabens on Mars and Venus: Dike emplacement and deflation of underlying magma chamber, *Proc. Lunar Planet. Sci. Conf. 31st*, abstract 1854.

Mège, D., A. C. Cook, E. Garel, Y. Lagabrielle, and M. H. Cormier (2002), Surface collapse and volcanic rifting on Mars, *Proc. Lunar Planet. Sci. Conf. 33rd*, abstract 2042.

Mège, D., A. C. Cook, E. Garel, Y. Lagabrielle, and M. Cormier (2003), Volcanic rifting at Martian grabens, *J. Geophys. Res.*, *108*(E5), 5044, doi:10.1029/2002JE001852.

Mitrofanov, I. G., M. L. Litvak, A. S. Kozyrev, A. B. Sanin, V. I. Tret'yakov, W. Boynton, D. Hamara, C. Shinohara, R. S. Saunders, and D. Drake (2003), Global distribution of shallow water on Mars: Neutron mapping of summer-time surface by HEND/Odyssey, *Proc. Lunar Planet. Sci. Conf. 34th*, abstract 1104.

Montesi, L. G. J. (1999), Concentric dike swarm and internal structure of Pavonis Mons (Mars), *Proc. Lunar Planet. Sci. Conf. 30th*, abstract 1251.

Moore, J. M. (1990), Nature of the mantling deposit in the heavily cratered terrain of northeastern Arabia, Mars, *J. Geophys. Res.*, *95*, 14,279–14,289.

Newsom, H. E., G. E. Brittelle, C. A. Hibbitts, L. J. Crossey, and A. M. Kudo (1996), Impact crater lakes on Mars, *J. Geophys. Res.*, *101*, 14,951–14,955.

Ogawa, Y., Y. Yamagishi, and K. Kurita (2003), Correction to "Evaluation of melting process of the permafrost on Mars: Its implication for surface features" by Yoshiko Ogawa, Yasuko Yamagishi, and Kei Kurita, *J. Geophys. Res.*, *108*(E7), 5071, doi:10.1029/2003JE002118.

Ormö, J., and G. Blomqvist (1996), Magnetic modeling as a tool in the evaluation of impact structures, with special reference to the Tvaren Bay impact crater, SE Sweden, *Tectonophysics*, *262*, 291–300.

Osinski, G. R., and J. G. Spray (2003), Complex crater formation and collapse: Observations at the Haughton impact structure, Arctic Canada, paper presented at Workshop on Impact Cratering: Bridging the Gap Between Modeling and Observations, Lunar and Planet. Sci., Houston, Tex.

Osinski, G. R., J. G. Spray, and P. Lee (2001), Impact-induced hydrothermal activity within the Haughton impact structure, arctic Canada: Generation of a warm, wet oasis, *Meteorit. Planet. Sci.*, *36*, 731–745.

Osinski, G. R., P. Lee, J. G. Spray, J. Parnell, D. Lim, B. Glass, C. S. Cockell, and T. E. Bunch (2005), Geological overview and cratering model for the Haughton impact structure, Devon Island, Canadian High Arctic, *Meteorit. Planet. Sci.*, in press.

Rodriguez, J. A. P., S. Sasaki, and H. Miyamoto (2003), Nature and hydrological relevance of the Shalbatana complex underground cavernous system, *Geophys. Res. Lett.*, *30*(6), 1304, doi:10.1029/2002GL016547.

Rodriguez, J. A. P., S. Sasaki, J. M. Dohm, K. L. Tanaka, H. Miyamoto, V. Baker, J. A. Skinner, G. Komatsu, A. G. Fairén, and J. C. Ferris (2004), Outflow channel sources, reactivation and chaos formation, XantheTerra, Mars, paper presented at Workshop on Hemispheres Apart: The Origin and Modification of the Martian Crustal Dichotomy, Lunar and Planet. Inst., Houston, Tex.

Rodriguez, J. A. P., S. Sasaki, R. O. Kuzmin, J. M. Dohm, K. L. Tanaka, H. Miyamoto, K. Kurita, G. Komatsu, A. G. Fairén, and J. C. Ferris (2005), Outflow channel sources, reactivation and chaos formation, Xanthe Terra, Mars, *Icarus*, in press.

Rotto, S., and K. L. Tanaka (1995), Geologic/geomorphic map of the Chryse Planitia region of Mars, 1:5,000,000, *U.S. Geol. Surv. Misc. Invest. Ser., Map I-2441-A*.

Schultz, P. H., and H. Glicken (1979), Impact crater and basin control of igneous processes on Mars, *J. Geophys. Res.*, *84*, 8033–8047.

Schultz, P. H., and A. B. Lutz (1988), Polar wandering of Mars, *Icarus*, *73*, 91–141.

Scott, D. H., and K. L. Tanaka (1986), Geologic map of the western equatorial region of Mars, 1:15,000,000, *U.S. Geol. Surv. Misc. Invest. Ser. Map, I-1802-A*.

Scott, D. H., J. M. Dohm, and J. W. Rice Jr. (1995), Map of Mars showing channels and possible paleolake basins, *U.S. Geol. Surv. Misc. Invest. Ser.*, *Map I-2461*.

Scott, E. D., and L. Wilson (2002), Plinian eruptions and passive collapse events as mechanisms of formation for Martian pit chain craters, *J. Geophys. Res.*, *107*(E4), 5020, doi:10.1029/2000JE001432.

Scott, E. D., L. Wilson, and J. W. Head (2000), Martian plinian eruptions and pit chain craters, *Proc. Lunar Planet. Sci. Conf. 31st*, abstract 1332.

Scott, E. D., L. Wilson, and J. W. Head III (2002), Emplacement of giant radial dikes in the northern Tharsis region of Mars, *J. Geophys. Res.*, *107*(E4), 5019, doi:10.1029/2000JE001431.

Sims, D. W., A. P. Morris, D. A. Ferrill, D. Y. Wyrick, and S. L. Colton (2003), Physical models of pit chain formation over dilational faults on Mars, *Proc. Lunar Planet. Sci. Conf. 34th*, abstract 2099.

Spencer, J., and F. Fanale (1990), New models for the origin of Valles Marineris closed depressions, *J. Geophys. Res.*, *95*, 14,301–14,313.

Spray, J. G. (1998), Localized shock- and friction-induced melting in response to hypervelocity impact, in *Meteorites: Flux With Time and Impact Effects*, edited by M. M. Grady et al., *Geol. Soc. Spec. Publ.*, *140*, 171–180.

Spray, J. G., and L. M. Thompson (1995), Friction melt distribution in a multi-ring impact basin, *Nature*, *373*, 130–132.

Spray, J. G., H. R. Butler, and L. M. Thompson (2004), Tectonic influences on the morphometry of the Sudbury impact structure: Implications for the terrestrial cratering and modeling, *Meteorit. Planet. Sci.*, *39*, 287–301.

Strom, R. G., S. K. Croft, and N. G. Barlow (1992), The Martian impact cratering record, in *Mars*, edited by H. H. Kieffer et al., pp. 383–423, Univ. of Ariz. Press, Tucson.

Tanaka, K. L. (1997), Origin of Valles Marineris and Noctis Labyrinthus, Mars, by structurally controlled collapse and erosion of crustal materials, *Proc. Lunar Planet. Sci. Conf. 28th*, abstract 1169.

Tanaka, K. L. (2000), Dust and ice deposition in the Martian geologic record, *Icarus*, *144*, 254–266.

Tanaka, K. L., and M. P. Golombek (1989), Martian tension fractures and the formation of grabens and collapse features at Valles Marineris (abstract), *Proc. Lunar Planet. Sci. Conf. 19th*, 383–396.

Tanaka, K. L., M. P. Golombek, and W. B. Banerdt (1991), Reconciliation of stress and structural histories of the Tharsis region of Mars, *J. Geophys. Res.*, *95*, 15,617–15,633.

Tanaka, K. L., J. A. Skinner Jr., T. M. Hare, T. Joyal, and A. Wenker (2003), Resurfacing history of the northern plains of Mars based on geologic mapping of Mars Global Surveyor data, *J. Geophys. Res.*, *108*(E4), 8043, doi:10.1029/2002JE001908.

Tanaka, K. L., T. Poruznick, J. A. Skinner, and T. M. Hare (2004), Geology of layered sequences in Arabia Terra, Mars (abstract), paper presented at Second Conference on Early Mars, Lunar and Planet. Inst., Houston, Tex.

Thompson, G. A. (1998), Deep mantle plumes and geoscience vision, *GSA Today*, April(T568), 17–25.

von Dalwigk, I. (2003), Fracture pattern in a complex impact structure—What can it tell us about crater collapse? A new look at the Siljan impact structure, paper presented at EGS-AGU-EUG Joint Assembly, Eur. Geophys. Soc., Nice, France.

Wilson, L., and J. W. Head (2001), Giant dike swarms and related graben systems in the Tharsis province of Mars, *Proc. Lunar Planet. Sci. Conf. 32nd*, abstract 1153.

Wilson, L., and J. W. Head III (2002), Tharsis-radial graben systems as the surface manifestation of plume-related dike intrusion complexes: Models and implications, *J. Geophys. Res.*, *107*(E8), 5057, doi:10.1029/2001JE001593.

Witbeck, N. E., K. L. Tanaka, and D. H. Scott (1991), Geologic map of the Valles Marineris region, Mars, *U.S. Geol. Surv. Misc. Invest. Ser., Map I-2010*.

Wyrick, D. Y., D. A. Ferrill, D. W. Sims, and S. L. Colton (2003), Distribution, morphology and structural associations of Martian pit crater chains, *Proc. Lunar Planet. Sci. Conf. 34th*, *34th*, abstract 2025.

Wyrick, D., D. A. Ferrill, A. P. Morris, S. L. Colton, and D. W. Sims (2004), Distribution, morphology, and origins of Martian pit crater chains, *J. Geophys. Res.*, *109*, E06005, doi:10.1029/2004JE002240.

Zhang, Y. (1998), Experimental simulations of gas-driven eruptions: Kinetics of bubble growth and effect of geometry, *Bull. Volcanol.*, *59*, 281–290.

Zhang, Y., B. Sturtevant, and E. M. Stolper (1997), Dynamics of gas-driven eruptions: Experimental simulations using CO_2-H_2O-polymer system, *J. Geophys. Res.*, *102*(B2), 3077–3096.

V. Baker, J. M. Dohm, H. Miyamoto, and B. Strom, Department of Hydrology and Water Resources, University of Arizona, Tucson, AZ 85721, USA.

A. G. Fairén, Centro de Biología Molecular, CSIC-Universidad Autónoma de Madrid, Cantoblanco, Madrid 28049, Spain.

J. Kargel and K. L. Tanaka, U.S. Geological Survey, Flagstaff, AZ 86001, USA.

G. Komatsu, International Research School of Planetary Sciences, 65127 Pescara, Italy.

K. Kurita, Earthquake Research Institute, University of Tokyo, Tokyo 113-0032, Japan.

R. Kuzmin, Vernadsky Institute, Russian Academy of Sciences, Kosygin St. 19, Moscow 119991, Russia.

J. A. P. Rodríguez and S. Sasaki, Department of Earth and Planetary Science, University of Tokyo, San Go Kan, 502 Shitsu, Tokyo 113-0033, Japan. (alexis1709@yahoo.com)

J. G. Spray, Planetary and Space Science Center, Department of Geology, University of New Brunswick, 2 Bailey Drive, Fredericton, NB, Canada E3B 5A3.